Position-controlled deposition for electrospinning

Solberg, R.H.M.

Award date:
2007

Position-controlled deposition for electrospinning

R.H.M. Solberg

DCT 2007.048

Master thesis

Coaches: dr.ir. M.J.G. van de Molengraft *
dr.ir. G.W.M. Peters **
prof.dr.ir. H.E.H. Meijer **

Supervisor: prof.dr.ir. M. Steinbuch *

Eindhoven University of Technology
Department Mechanical Engineering

* section Control Systems Technology (CST)

** section Material Technology (MaTe)

Eindhoven, May, 2007

Preface

This report describes the results of my graduation project at the Control Systems Technology group and (partially) the Material Technology group at the department of Mechanical Engineering of the Technische Universiteit Eindhoven. Over 18 months ago this project started as a great jump into unknown territory for me and a great challenge of exploring a new field of interest for the above mentioned research groups. During my graduation period it has become clear that the field of electrospinning requires a multidisciplinary approach which cannot be managed by one person. Herewith I therefore would like to show my gratitude to the persons who have helped me with my research during the graduation period.

In first place, I would like to thank my coaches Gerrit Peters and René van de Molengraft for their encouraging discussions and support. You have also given me great freedom in determining the course of my research.

In second place, I would like to thank Rint Sijbesma for providing the temporary experimental setup and Eva Wisse for helping me with the spinning materials. Sjef Garenfeld for creating the small experimental setup and Harrie van de Loo for all the 'techtalk' and computer facilities. Marc van Maris and Lambert van Breemen for the microscopic imaging at the multiscale laboratory and Rafael Wilkosz for the special digital pictures.

In third place, Martien Hulsen and Peter Roozemond for digging through the model evaluation part with me.

Special thanks goes to Jan van Heerebeek and Jovita Moerel of the GTD for their support with the creation of the new spinning cabin and the CE certification. You really make amazing stuff with a great eye for detail!

Finally, I would like to show my gratitude towards my parents and girlfriend Twannie, for their great support during almost seven years of studying, and for having great patience with the workaholic I often seem to be.

Ramon Solberg

Abstract

Electrospinning comprises an efficient and versatile technique for the fabrication of very thin fibers from a rich variety of materials including polymers, composites and ceramics. The process provides opportunities for the relatively easy fabrication of micron-scaled parts or parts with nano-scaled details. During the recent years it has regained more and more attention due to the surging interest in nanotechnology. Potential applications range from filter media to tissue engineering scaffolds and many others.
The still remaining problem with electrospinning is the unstable deposition of the fiber, creating nonwoven fabrics. These fabrics have varying characteristics and many studies have been done to solve this problem by making the fiber deposition controllable. With this ability geometric complex structures could be woven with in advance defined characteristics.

A recent finding has presented a method which could fulfill these wishes. This founding (patented by Eindhoven University of Technology) comprises the use of a small, positionable ground point for focussing the fiber deposition. The goal for this research study was to show the 'proof of principle' of the founding and the development of all the necessary equipment.

A study of the electrospinning process has indicated the need for two special experimental devices. A dedicated electrospin cabin has been designed and created to meet the safety regulations. Another experimental setup (a spiral spinner) has been built to investigate the influence of the collecting speed on the focussing of the fiber.

Experiments with this setup have shown that the alignment of even one single fiber is feasible. An accompanying remarkable observation is the stabilization of the fiber deposition which occurs at higher collecting speeds. Visualizations of the process, made by a high speed imaging camera, have shown that the instability indeed fades out. Although some papers report similar results, the alignment of one single fiber in a large, one dimensional space together with a stabilized deposition has not been reported yet. The visualizations however, also show the bending of the fiber into a curved shape above the deposition target, resulting in a large positioning error. In the near future, this error might be reduced by the miniaturization of the spinning process. A model description of this bending fase might also attenuate this error because the control system can be adapted by the predicted error

from the model. As a starting point for this description a model has been evaluated which describes the radial reduction of the fiber diameter for newtonian polymer solutions. This result can be used for subsequent modeling studies on the bending of the fiber.

Samenvatting

Electrospinning is een efficiënte en universele manier om zeer dunne vezels te fabriceren uit een rijke hoeveelheid materialen zoals polymeren, composieten en keramieken. Het proces biedt mogelijkheden om relatief makkelijk onderdelen met kleine dimensies te vervaardigen (op micron en/of nano schaal). De laatste jaren heeft dit proces een toenemende aandacht verworven door de snel groeiende interesse in nanotechnologie. Toepassingen hiervoor lopen uiteen van filter materialen tot tissue engineering scaffolds en nog vele anderen.
Het bestaande probleem bij het electrospinnen is de instabiele depositie van de vezel, welke zorgt voor de creatie van zogenoemde 'nonwovens' ofwel niet geweefde stukken weefsel. Deze weefsels bevatten variabele karakteristieken en om dit probleem op te lossen zijn er vele onderzoeken verricht naar het positioneerbaar maken van de vezel depositie. Met deze kundigheid kunnen uiteindelijk geometrisch complexe structuren worden gemaakt, met vooraf opgegeven eigenschappen.

Een nieuwe uitvinding, die recentelijk gepatenteerd is door de Technische Universiteit Eindhoven, biedt een methode om dit mogelijk te maken. Het omvat een klein, positioneerbaar (geaard) punt om de vezel depositie te focusseren. Het doel van dit onderzoeksproject is het aantonen van de haalbaarheid van de vinding en het ontwerpen en creëren van de bijbehorende testapparatuur.

Een studie naar het electrospinning proces heeft uitgewezen dat er twee testopstellingen nodig zijn voor het verdere onderzoek. Om aan de vereiste veiligheids aspecten te voldoen is er een speciale spincabine ontworpen en gemaakt. Een andere opstelling (een spiraal spinner) is gemaakt om de invloed van de opwind snelheid op de focussering van de vezel te onderzoeken.

Experimenten met deze opstelling hebben aangetoond dat een rechtlijnige depositie van de vezel haalbaar is. Een bijkomende opmerkelijke waarneming is de stabilisatie van de vezel depositie bij hogere (opwind) snelheden. Visualisaties van dit proces, welke zijn gemaakt met behulp van een hogesnelheidscamera, hebben uitgewezen dat de stabilisatie van de vezel daadwerkelijk plaatsvindt. Hoewel sommige publicaties overeenkomstige resultaten rapporteren, is het rechtlijnig neerleggen van de vezel in een groot vlak samen met een gestabiliseerde vezel depositie is nog niet beschreven in de literatuur. De visualisaties hebben echter ook een kromming van de vezel boven het depositievlak aangetoond. Dit ontstaat bij hogere

opwind snelheden en resulteert in grote afwijkingen in de positionering. In de nabije toekomst zou deze fout kunnen worden gereduceerd door miniaturisering van het spinproces en/of door een modelmatige beschrijving van de vezelkromming. Als startpunt voor deze beschrijving is een model geëvalueerd welke de radiale reductie van de vezeldiameter beschrijft voor newtonse polymeer oplossingen. De uitwerking van dit model kan worden gebruikt voor de opvolgende modelonderzoeken naar het krommen van de vezel.

Contents

1

Introduction

1.1 Motivation

Electrospinning is an efficient and versatile technique for the fabrication of very thin fibers from a rich variety of materials including polymers, composites and ceramics. This technique offers an approach in creating nanofibers with both solid and hollow interiors. The resulting fibers have a large length, are uniform in diameter and may consist of diverse compositions. The creation of a fiber via electrospinning is based on the uniaxial elongation of a viscous or viscoelastic jet which is derived from a polymer solution or melt. The technique is very similar to commercial processes for drawing small diameter fibers, except for the use of electrostatic repulsive forces (instead of mechanical forces) between two or more charged surfaces. These forces continuously stretch the jet reducing its diameter. In contrast to mechanical drawing processes, fiberspinning through the application of an external electric field provides a contactless 'drawing' scheme which provides the ability to produce fibers with much thinner diameters.

The first electrospinning trials were already made in the 1930's and the first patents were issued by Formhals [1, 2, 3, 4, 5] from 1934 to 1944. He outlined different experimental setups for the production of polymer filaments using electrostatic force. An example of these setups can be seen in figure 1.1. A polymer solution, which was ejected out of a metal spinnerettes with a small hole, was introduced into an electric field. Polymer filaments were formed between two electrodes bearing electric charges of different polarity. One of these electrodes was placed into the solution (spinnerettes) and the other was placed under a moving collector. It was found that the necessary potential difference to initiate the process depended on the properties of the solution, such as the molecular weight of the polymer and the viscosity of the solution. Also by shortening the distance between the spinnerettes and the collector it was found that the spun fibers tended to stick to the collector as well as to each other, due to incomplete evaporation of the solvent.

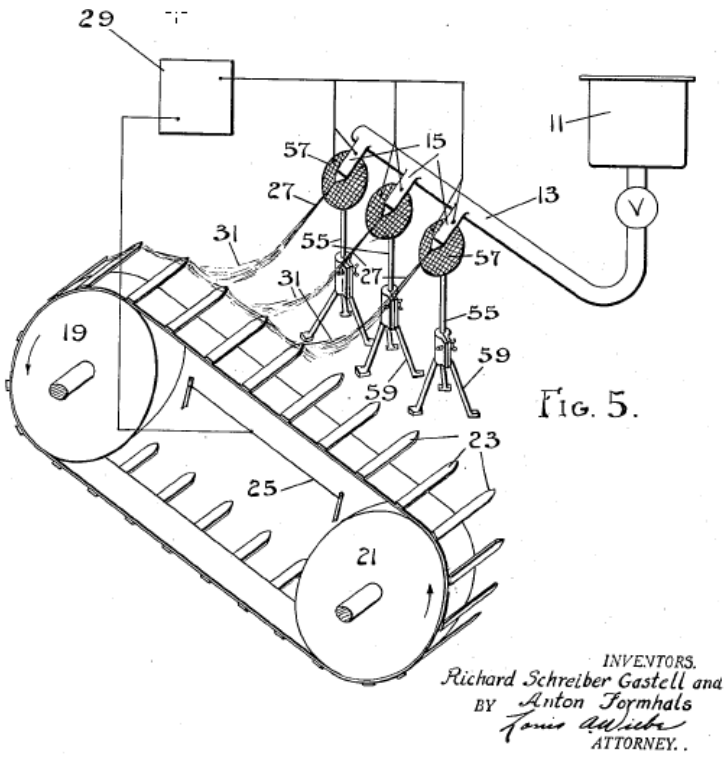

Figure 1.1: One of the sketches in the patent of Formhals from 1934 [1]

Up until the early 1980's only a handful publications covering this subject emerged, but during the mid 1980's, and even more during recent years, electrospinning has gained more and more attention. The main cause of this revived interest is probably due to the surging interest in nanotechnology and just this process providing opportunities for the relatively easy fabrication of micron-scaled parts or parts with nano-scale details. Strangely enough, how promising the electrospinning process might seem to be, its understanding is still very limited.

1.2 Application areas

The small diameter of the resulting fibers (ranging from a few nanometers to a few microns) is the most important characteristic of the proces. Fabric's made from nanofibers can, for example, be used for the filtration of submicron particles in the air treatment industry [6, 7]. The reinforcement of advanced composites by using electrospun fibers also shows promising results [8]. Other applications lie in the medical field, such as wound dressing (e.g. burns), tissue engineering scaffolds [9, 10], the creation of artificial blood vessels [11] and even regenerative medicine with encapsulated living cells [12]. Also the possibilities for using nanofibers for the fabrication of micro- and nanodevices have not remained unnoticed. Some examples are field effect transistors [13], gas and optical sensors [14, 15].
More extended or perspective application areas are summarized in the papers of

Z.M. Huang et al. [16] and D.Li, Y.Xia [17], See also figure 1.2. It should be noted that most of these applications are accomplished in a laboratory research stage. Many of them have high promising potential, but only a few have reached industry level application jet.

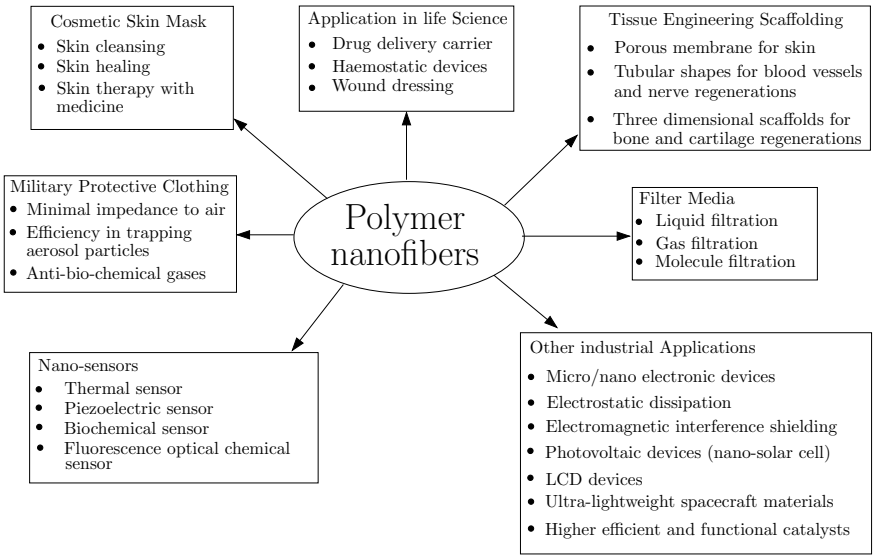

Figure 1.2: Potential applications of electrospun polymer nanofibers [16]

1.3 Problem statement

Most (future) applications wherein electrospun fibers are used are based on so-called 'nonwoven' fabrics. During fabrication the substrates (moulds), for the creation of for example submicron filters or medical scaffolds, are being grounded or given a certain potential as a whole. A key occurrence during the formation of submicron fibers is a convective instability in the elongating jet [18]. The jet will start rapidly whipping as it travels towards the collector. Therefore, during the electrospinning process, the whole substrate is covered with a layer of randomly placed fiber. The created fabric (see figure 1.3) has a chaotic structure and it is difficult to characterize its properties. For instance for a filter the pore-size is of great importance (because of the filter grade and the flow resistance) and for instance for medical applications the pore-size is of great importance because of cell ingrowth. To fabricate micro- and nanodevices, mostly not a whole fabric but only a single straight fiber or a fiber woven in a specific form is desired.

Therefore, many studies have been done to make the fiber deposition controllable. By controlling the point of deposition, the oscillating effect of the elongating fiber might be reduced and its location could be guided into every desired direction. With this ability geometric complex structures could be woven with for instance a desired pore-size and/or thickness. Also parallel straight fibers could be woven for

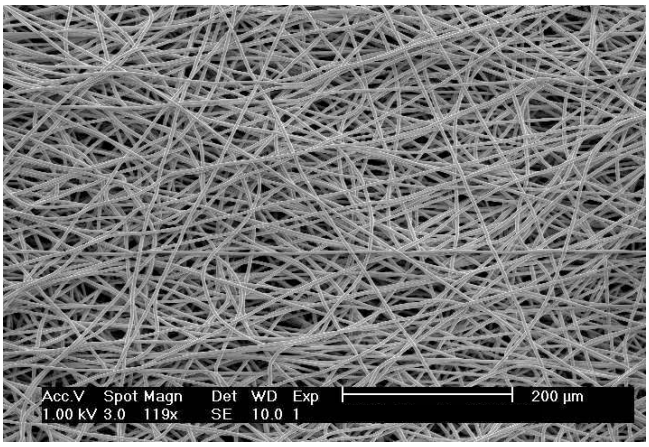

Figure 1.3: SEM micrograph of an electrospun nonwoven fabric

usage in micro- an nanodevices.

A recent founding has shown that by using a small ground point, instead of grounding the whole mould, the sub-micron fiber deposition can be focussed. This founding has been patented [19] by Eindhoven University of Technology and needs further research and development. The foundation of this research can be extracted from [19] as:

Investigate the new found procedure(s) for the fabrication of a sub-micron fiber (out of a specific material) with the use of an electric field, by which the fiber deposition point, during the fabrication process, is position controllable.

In the patent [19] two different procedures are elaborated. The first uses a needle shaped electrode at the deposit side which can be moved in a certain space, with a proper mechanical support system, to guide the deposit position of the fiber over a collecting surface. The other procedure utilizes a matrix like set-up of different electrodes at the deposit side which form a sort of co-ordinate system. Herewith every electrode should be switchable to a certain potential in time to guide the fiber deposition onto a desired location.
The main goal of this research study is to produce the '*proof of principle*' of the new, patented founding. To investigate these two procedures, first of all the electrospinning process itself must be thoroughly investigated and a user friendly spinning material has to be chosen. Next the focusing process on a small electrode can be investigated and predictions can be made about the feasibility of the founding.
Subsequently, experimental test equipment has to be developed to further investigate the above mentioned procedure(s). Also an electrospinning set-up (cabin) has to be built in which the experimental test equipment can be (safely) utilized. The equipment should give more insight in the achievable position accuracy and nature of the spun fiber. This is important because it gives an answer to the question of how accurate (geometric complex) structures eventually could be woven. The problem statement for this research study may now be summarized into the following:

Elaborate the new patented electrospinning procedure(s) to show the 'proof of principle' and develop all necessary equipment to gain insight in the achievable accuracy and nature of the spun fiber.

If the final research results are satisfactory, new applications can be developed together with the wishes of e.g. the air treatment industry or the medical industry. This should, finally, lead to new pioneering spinning machines which are able to make woven fabrics or straight single fibers according to the specifications of the final user (or customer).

1.4 Outline of the report

The next chapter presents the basic investigation of the electrospinning process. Next to the process description , a brief overview of the possible spinning solutions and deposit materials will be elaborated. The electric field behaviour is investigated and feasibility tests are executed to study the possibilities of the new founding.
Next, new, specialized instruments for further experimentation have to be designed. This comprises the design of a new, safety approved spinning cabin and the design of fiber collecting devices. All this is presented in Chapter 3.
In Chapter 4 the use of these instruments is described and the results are discussed. The spinning process is visualized by using a high speed imaging camera. This provides a better interpretation of the achieved results.
Chapter 5 presents the take-off point for a model based interpretation for the estimation of the positioning error. The (future) elaboration of this model should give the amount of fiberbending to predict the true position of deposition. This model can possibly improve the spinning accuracy.
Based on the results, conclusions are drawn and possible assignments for future work are extracted. This is done in Chapter 6.

2

Electrospinning - The Basics

2.1 Introduction

The basics of the electrospinning process are presented followed by a brief overview of usable spinning materials and intermediate deposit materials. Next, a brief analysis of the electric field behaviour is included. At last a feasibility study of the new founding is presented and discussed.

2.2 Process Setup

In Fig. 2.1 an example of an ordinary experimental electrospinning setup is shown. The syringe, which contains the polymer solution, is placed in a metering pump to generate a constant pressure and flow of the fluid through the needle. A high voltage source is attached to the needle and the grounded collector to create an electric field between these two points. Mostly Direct current (DC) supplies are used although the use of Alternating Current (AC) supplies is also feasible [20]. The voltage source generally has an adjustable range of 0 to $\pm$ 30 kV.

The applied voltage induces a high electric charge on the surface of the solution-drop at the needle tip. The drop now experiences two major electrostatic forces: The coulombic force which is induced by the electrical field, and electrostatic repulsion between the surface charges. The intensity of these forces causes the hemispherical surface of the drop to elongate and form a conical shape, which is also known as the Taylor cone [21]. By further increasing the strength of the field, the electrostatic forces in the drop will overcome the surface tension of the fluid/air interface and an electrically charged jet will be ejected.

After the ejection, the jet elongates and the solvent evaporates, leaving an electrically charged fiber which, during the elongation process, becomes very thin. The characteristic feature of this process is the onset of a chaotic oscillation of the elongating jet which is due to the electrostatic interactions between the external electric field and the surface charges on the jet as well as the electrostatic repulsion of

mutual fiber parts [17, 22]. The fiber can be spun directly onto the grounded (conducting) screen or on an intermediate deposit material. Because of the oscillation, the fiber is deposited randomly on the collector, creating a so called 'non-woven' fiber fabric.

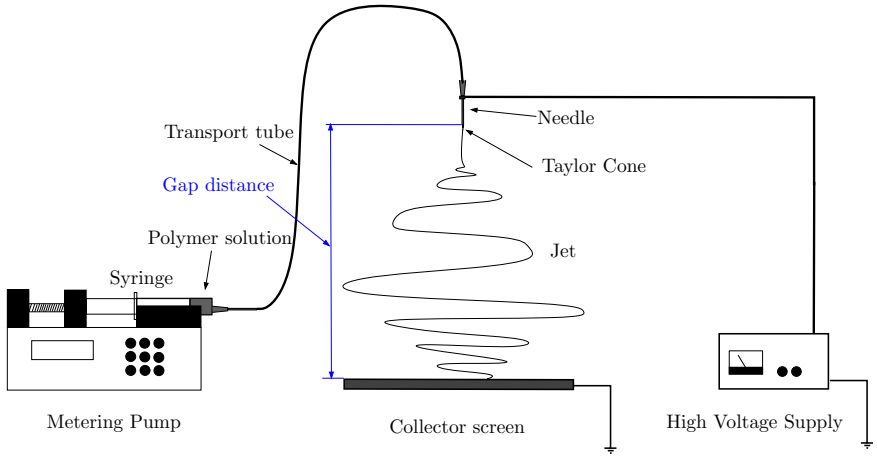

Figure 2.1: Schematic of an ordinary electrospinning setup

2.3 Processing parameters, materials and control

2.3.1 Parameters

A number of parameters influence the nature and diameter of the electrospun fibers which are produced by the above described process. These parameters include [16, 17, 23]:

Material parameters:

- Molecular weight, Molecular-weight distribution and architecture (branched, linear, etc.) of the polymer
- Solution properties (viscosity (concentration), conductivity and surface tension)

Operational parameters:

- Electric field strength and feeding rate
- Distance (gap) between the tip and collection screen
- Ambient parameters (temperature, humidity and air velocity in the chamber)

2.3.2 Materials

Spinning materials

In open literature more than fifty different polymers can be found which have been successfully electrospun into small fibers with diameters ranging from a few nanometers to a few micrometers. This can be polymer solutions as well as polymer melts. The solutions are usually made by dissolving polymer pellets or powder in a specific solvent. This process as well as the electrospinning of these solutions is essentially conducted at room temperature with atmospheric condition. Many of the polymer solutions emit harmful or at least very unpleasant fumes, and therefore the spinning process must always be conducted within chambers with a dedicated ventilation system (fume cupboard).
Polymer melts are created by melting a polymer with a high temperature source and putting it in a (heated) capillary tube. The difference between the spinning processes is that the spinning of melts must be conducted in a vacuum environment [16]. Because of the difficulty of creating the whole spinning setup in a vacuum chamber, much less polymer fibers have been produced this way.
An extensive summary of spinnable polymer solutions and melts is listed in table 1 of [16]. This table also gives the solvents that can be used and the accompanying polymer concentrations. Its also worth noting that many polymers can be dissolved in different solvents or solvent combinations.
According to the paper of D.Li and Y.Xia [17] a variety of methods have recently been developed to (again) increase the diversity of spinnable materials. These methods are capable of generating materials out of specific chemical compositions. They therefore provide various biological, optical, magnetic and electronic properties. A combination of these functionalities in one sample to create multifunctional fibers should also be feasible. The materials which have been used in this study are polymer solutions only, see Table 2.1. Spinning the polycaprolactone (PCL) solution is accompanied with harmful chloroform fumes and has therefore only been conducted during the first spinning trials. The polyethylene oxide (PEO) solution is by far the most used material in electrospinning studies and relatively simple to prepare. Because of this, most of the research is performed using this material.

Table 2.1: Used spinning materials

Polymer	Mol. weight	Solvent	Concentration
PCL (Polycaprolactone)	200,000	Chloroform	17 wt%
PEO(Polyethylene oxide)	400,000	Distilled water / Ethanol (2:3)	4-9 wt%
PVA (Polyvinil alcohol)	65,000	Distilled water	8-16 wt%

Deposit materials

For collecting the fiber, an intermediate deposit material can be used. This material should be a thin isolator in order to diminish the disturbance of the electric field. Appropriate materials are, for instance, a pvc sheet (A4 transparencies), a polyester sheet (Mylar) or a thin sheet of glass. A polyester sheet has a larger isolation value than a PVC sheet and is usually available as a foil

which is used for instance as the isolation medium within copper coils. After the spinning process, these films can easily be inspected under a microscope or even be sputter coated for investigation in a SEM.

2.3.3 Control

In section 2.3.1 the parameters that influence the nature and diameter of the resulting fiber have been presented. Obtaining the ability to control these features is still a major challenge in the field. Ideal functionalities would be: (1) the diameter of the fibers to be controllable and uniform, (2) the surface of the fiber to be defect-free and (3) that a single continuous fiber would be collectable. Considering the many publications which cover these subjects, it is demonstrated that these functionalities are (still) difficult to achieve.
One of the appearing problems during electrospinning is the formation of beads (see Fig. 2.2) on the resulting fibers. Several researchers (as e.g. the group of Reneker [24]) have identified that the density of beads can be decreased or even wiped out by increasing the viscosity of the polymer solution. Also adding salts to the solution can lead to the same result. This because of the increase in the net charge density of the solvent. It is also found that the strength of the electric field influences the formation of beads. By changing the field strength (voltage level) the conical shape of the solution drop (at the needle tip) is also influenced. If the drop is not transformed into a Taylor cone-shape, the ejecting fiber might be unstable which results, again, in the formation of beads.
Besides avoiding the formation of beads, the control of the fiber diameter itself can be affected by the solution concentration, the electric field strength, the feeding rate at the needle tip and the gap between the needle and the collecting screen. The properties of the used polymer and the ambient parameters are difficult to change during the process and therefore mostly considered to be steady. In Fig. 2.3 a schematic overview (presented by G. Wilkes [23]) of the most influencing parameters and their effect on the diameter is presented.

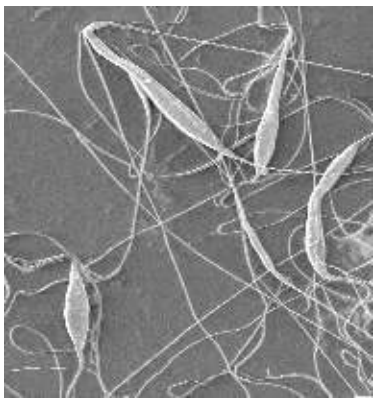

Figure 2.2: SEM image of PEO fibers containing beads

An increase of the gap distance gives the fiber more room to stretch and results in a smaller diameter. By increasing the feeding rate a larger volume of solution is spun into a fiber which results in the formation of larger diameters. More

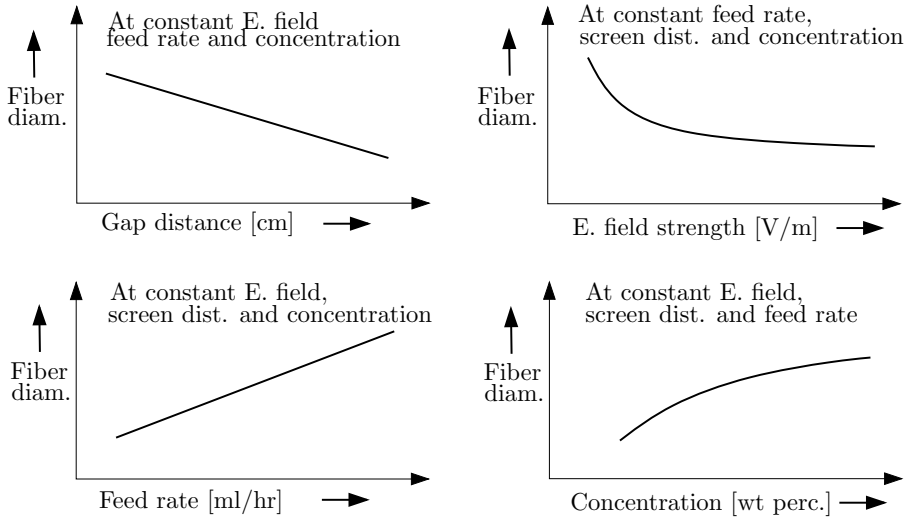

Figure 2.3: Effect of process parameters on fiber diameter [23]

concentrated solutions also give thicker fibers. By using a higher electric field strength it is believed that the whole elongation process is speeded up (greater forces) which results in a smaller fiberdiameter. But, as stated before, changing the strength of the field may also have negative effects. The figure, as it is presented here, only shows the influence if only one parameter is changed. The whole process however may be characterized as depending on the interplay of al these factors together.

2.4 Feasibility study

Patent [19] describes two different approaches for focussing the fiber deposition. Both approaches attempt to replace the grounded collecting plate with a very small grounded electrode. The first approach concerns a small needle shaped electrode which should be moved in a certain space (2.4 (a)) and the other approach concerns many stacked electrodes in a matrix like setup in which every electrode is individually switchable to the ground point (2.4 (b)).
The second method only differs from the first in not having a moving electrode. The movement is now achieved by switching over to an adjoining electrode in a specific direction. The great advantage of this method is having no moving parts in the setup which are liable to wear. Nevertheless it can be concluded that the basic idea of grounding a small electrode is incorporated in both methods, so elaborating only the first method will cover both approaches.

2.4.1 FEM analysis

In order to gain insight in the alteration of the shape and influence of the electric field, by the change in the setup, a Finite Element analysis has been carried out (using FemLab 3 [25]). The analysis of the original situation, with a grounded plate

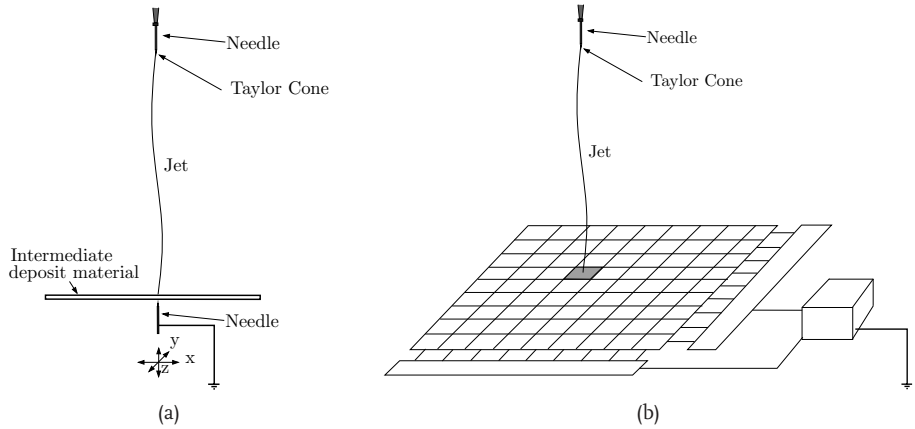

Figure 2.4: Sketchy interpretation of the patented methods. (a) Represents the first approach by using a grounded movable needle shaped electrode and (b) represents the approach of a matrix like setup of individually switchable stacked electrodes.

at the bottom and the charged syringe needle at the top, is represented in Fig. 2.5 a. The horizontally oriented contour lines in the picture represent the equipotential lines of electrostatic potential. Perpendicular to these lines the shape of the electrostatic field (pulling force) is shown by red arrows. Four drawn blue streamlines emphasize that the force converges to the whole surface of the grounded plate.
When the plate is replaced by a grounded needle (Fig. 2.5b) , the flow of the electric potential is concentrated and therefore the electrostatic force will converge towards the needle. Again four drawn streamlines emphasize the convergence of the forces to the needle shaped electrode. Fig. 2.5c represents a surface plot of the electric field strength on the bottom of the setup. Blue indicates a weak strength whereas red indicates a very strong field strength. The figure clearly shows that the point of the needle will exert the greatest pulling force on the jet.
It can now be concluded that changing the setup from a grounded plate to a grounded needle has a large effect on the electrostatic field. The pulling forces converge to the needle which indicates that the spun fiber will converge towards this point. By also using a conical shaped tip the greatest pulling force is concentrated on this tip which means that the fiber might even be directed to the upper point of the needle. This phenomenon indicates a possibility for achieving good positioning accuracies. Similar observations have also been reported for a vertical, tapered disc by Theron et al. [22].

2.4.2 Experimental verification

The FEM analysis has clearly pointed out that the proposed electrospinning procedure concentrates the electrostatic forces and therefore indeed might induce positioning convergence of the deposited electrospun fiber.
In order to verify these findings a simple electrospinning test setup has been created. A cubic Lexan protection cover with a door has been made and a stand is placed within (see figure 2.6). The upper part of the stand is equipped with a truncated injection needle and on the bottom a plate or a needle electrode is

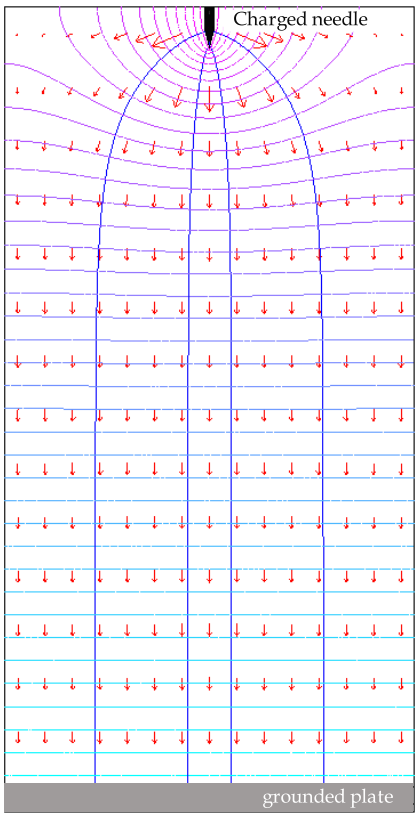

(a)

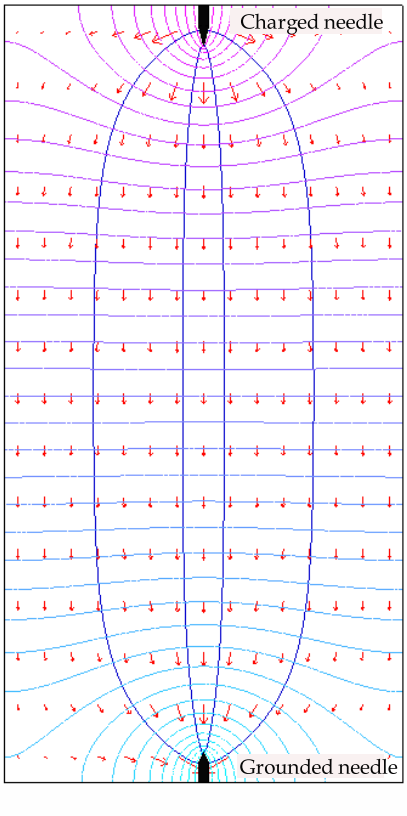

(b)

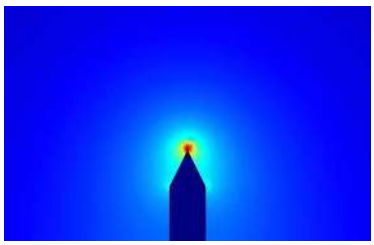

(c)

Figure 2.5: Electrostatic field simulations made with FemLab. (a) The equipotential lines of electrostatic potential are plotted with perpendicular to these lines the shape of the electrostatic forces (red arrows and blue streamlines). (b) represents the same plot, but with the grounded plate replaced by a grounded needle.(c) surface plot of the electric field strength on the bottom of the setup. Blue indicates a weak strength whereas red indicates a very strong field strength.

positioned. A laboratory high voltage source (Wallis VCS 303/1) is connected between the two electrodes and an infusion pump (Harvard PHD 2000) is used to feed the upper needle with the polymer solution via a teflon tube.

Figure 2.6: Electrospinning test setup

The verification tests have been performed at room temperature ($20°C$) in a fume cupboard, with the materials earlier discussed in section 2.3.2. A vertical distance between the electrodes of $120 - 150mm$, an electric potential of around $12 - 16kV$ and a flow of around $17\mu L/min$ creates a stable taylor cone with a continuously ejecting fiber. Small mylar sheets (cutout of 0.01mm thick mylar foil) are used for the collection of the fiber.
The first test has been done in the conventional way using a grounded plate. After the jet is ejected from the cone in a straight way, it starts to diverge and an oscillating haze can be seen above the plate. As a result the whole plate is covered with randomly deposited fiber and indeed a nonwoven fabric is created. An image of the result is presented in figure 2.7 a.
The second test has been done using a grounded (conical pointed) needle on which again a piece of sheet has been placed to collect the fiber. Now the same phenomenon takes place but the instability (haze of whipping fiber) seems to develop much slower. As a result the fiber is first collected exactly above the tip of the needle but in time this deposit spot starts to grow into a slowly increasing circular deposit area (see figure 2.7 b). This phenomenon can be explained by the fact that the fiber, which has been deposited on the sheet, retains an amount of residual charge which is sufficient enough to exert a repellent force. Therefore, after the first fiber part has been collected the continuous deposition enforces stacking up of fiber material on one location which eventually enforces the fiber to buckle. The already deposited fiber will exert a force on this new fiber and so 'sweep' this fiber to another location. As more fiber is collected the repellent forces

will constantly direct the depositing fiber further out of the center which results in a slowly growing circular deposit area. It remains circular because the grounded needle still exerts a force on the above depositing fiber. If this process is continued for a longer time, the sheet will be covered with a large circular nonwoven fabric.

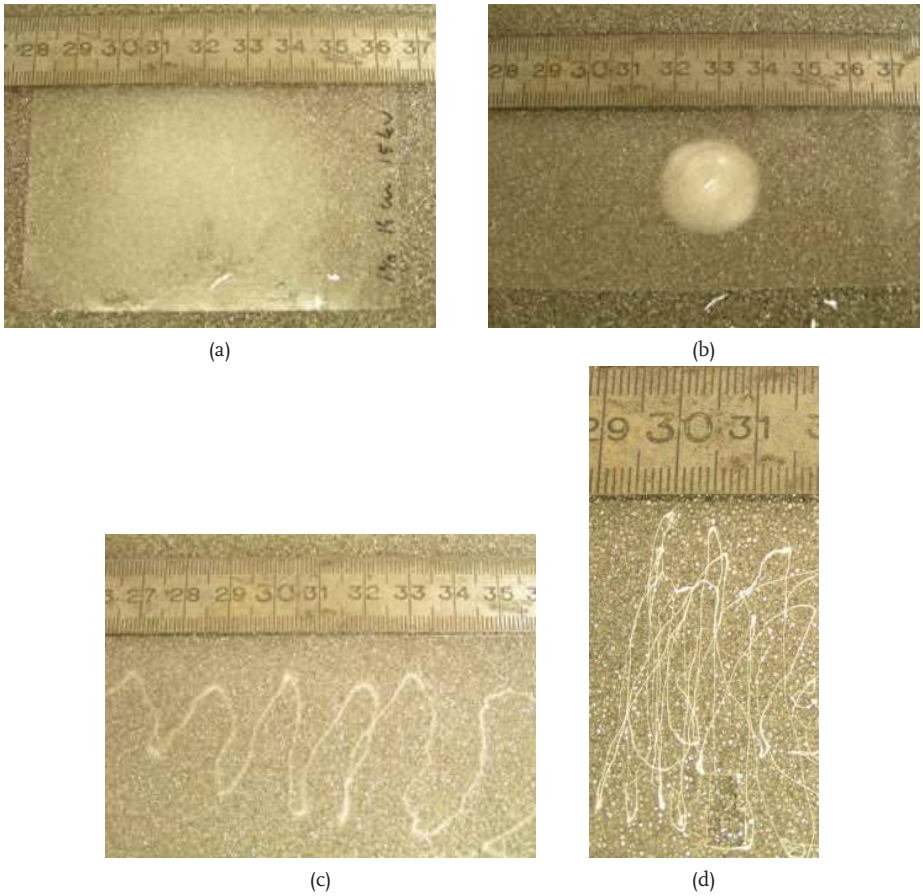

(a) (b) (c) (d)

Figure 2.7: 'Writing' samples

This test has clearly indicated that focussing of the deposition indeed occurs to the tip of the needle. Only this occurrence is of short duration. A way to work around this problem is to move the deposited fiber away from the grounded point. By moving the repellent forces away, the depositing fiber will stay attracted to the tip of the needle and focussing is maintained.
This has been done in the third test. By making a wavey movement with the sheet during the experiment the convergence is indeed maintained and a sort of written line of fiber is created (see Fig. 2.7 c). It can be noticed that at the peaks of this sinusoid the deposition is a little wider. This is explained by the fact that the traveling speed of the sheet is somewhat slower at these points and as a result a larger amount of fiber will be deposited on one location. This then will create greater repellent forces and the deposition area will become wider again.

With the sheet traveling speed being an important parameter, the last test has been performed with a faster wavey movement. The result is presented in Fig. 2.7 d. At a higher traveling speed, less material is deposited on the same location and less repellent forces are exerted on the deposition point. This results in a thinner line of spun fiber. In Fig. 2.8 microscopic images of two areas on the sheet are presented. The fiber is nicely entwined into a quite uniform porous thread. Fig. 2.9 presents a SEM image which shows that the fiber entwining is of proper quality and the thread has an average thickness of $200\mu m$.

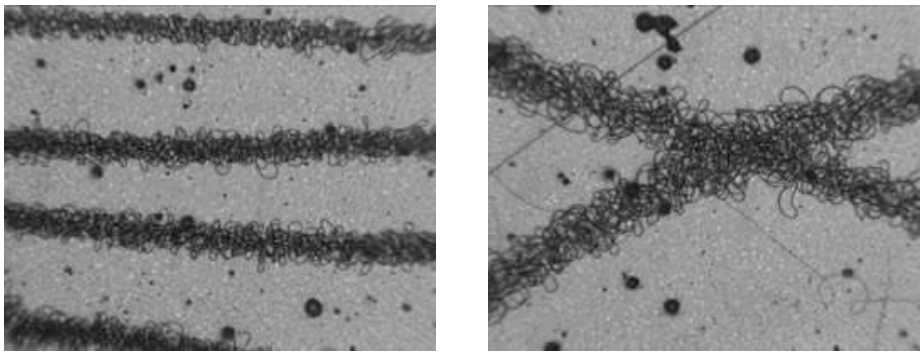

(a) (b)

Figure 2.8: Microscopic images of two areas on the sheet from the last feasibility test

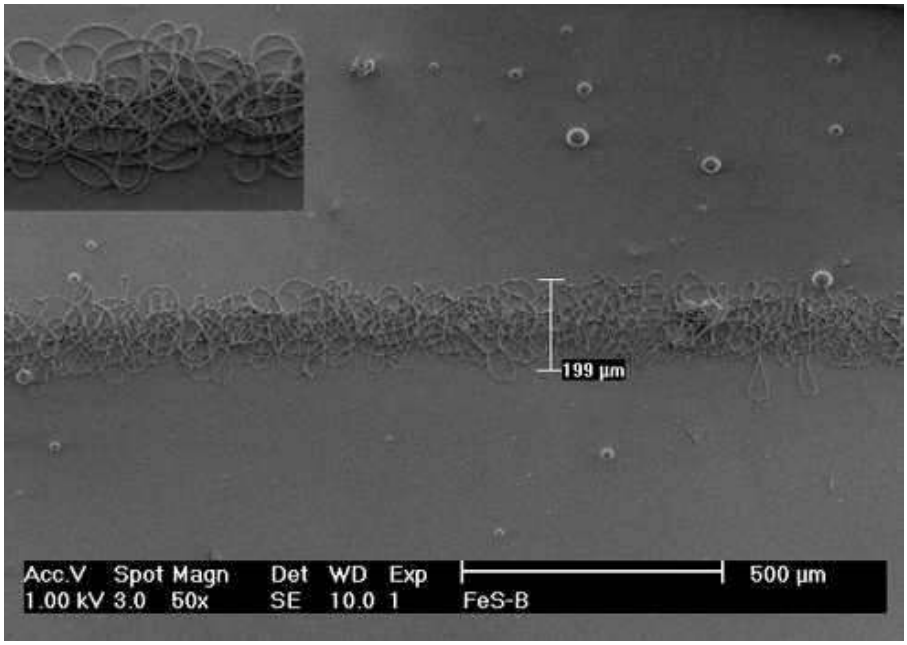

(a)

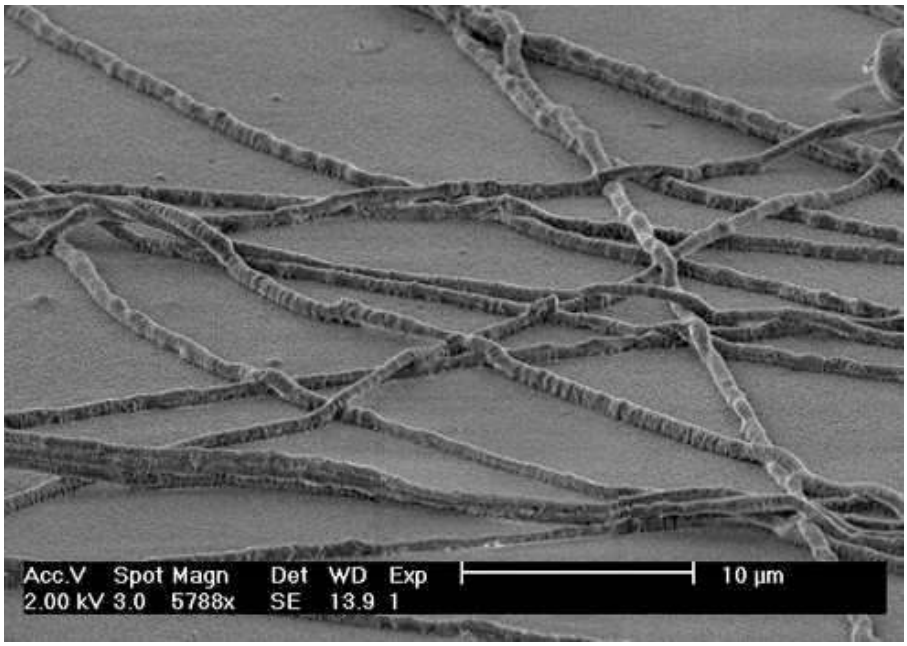

(b)

Figure 2.9: SEM images of a small part of the sheet from the last feasibility test

This last test indicated that the focussing process on a grounded needle can become rather accurate and it may be concluded that the elaborated procedure shows much potential. During the tests the sheet has been moved manually and

therefore the movement could not be done very precise and with great speed.
To bring this investigation to a higher level a dedicated spinning setup, containing a new controllable spinning cabin and a motion controlled setup, will have to be developed. These new setups should provide the ability to observe and control the focussing process of the fiber deposition more profoundly.

3

Experimental test equipment design

3.1 Introduction

Promising results concerning the focussing possibilities using a grounded needle were found. To continue the further development of the process, special instruments have to be designed. In this chapter the development and building of these instruments will be presented.

3.2 Electrospin cabin design

Electrospinning is a process which needs special safety regulations. During the spinning process the solvent evaporates from the elongating jet and possibly harmful fumes may escape from the setup. Another risky item is the high voltage. The accompanying current running through the setup can rise to a few micro Ampères. These values are harmful for the human body because any untimely contact, during operation, may affect the heartbeat, possibly resulting in death. Other aspects of using a high voltage between two electrodes with an airgap in between is the creation of ozone and röntgen radiation.
A new electrospinning setup has been designed with a protective cover of PMMA (see Fig. 3.1), the transparency of which yields a clear view on the process, while any direct contact is prevented. The roof is fitted with an exhaust pipe which is connected to the laboratory ventilation system and so, all escaping fumes are safely transferred away from the setup and its operator.
The cover is also equipped with a protected door. When the door is opened during operation, magnetic sensors are triggered and the whole system will be shutdown within a few microseconds. This makes any human contact with live charges virtually impossible. The setup is able to deliver up to $25kV$ and a study in cooperation with the central workshop (Gemeenschappelijke Technische Dienst, GTD) has shown that the level of röntgen radiation which arises within the current configuration is not harmful.
The control unit for the whole cabin is a Siemens PLC system, operated by an OP (Operating Panel). This panel is placed on the left side of the door at eye level. It

allows the operator to control several aspects of the spinning process as e.g. the spinning voltage, the infusion pump and timer controlled operation. The panel also provides information about the internal cabin temperature and flowing current through the High Voltage source. The flowing currents are in the range of a few hundred nanoampères and a special amplifier has been designed to provide the ability to measure these low values.
The PLC system can very easily be extended in the future to provide additional control of process features. An ethernet module will soon been added through which the PLC system can be controlled from Matlab or any other control environment. This will make the whole system, including added experimental systems, controllable from a single computer.
The cabin also has a double bottom in which all the electrical components have been concealed. This space also has a forced ventilation system to prevent heating up the rest of the cabin because of heat transfer through the bottom. This bottom has been made of a 30 mm thick PVC plate to isolate most of the electrical radiation between the two spaces. This should reduce the possible influence on the spinning process by the other electrical components and vice versa.
The finally created cabin (see figure 3.2) has gone through several safety and durability tests (by the GTD) and together with the composed technical construction file it has acquired full CE certification. The instruction manual can be found in Appendix A (in Dutch). All The technical drawings, operating instructions and CE declarations can be found in the technical construction file.

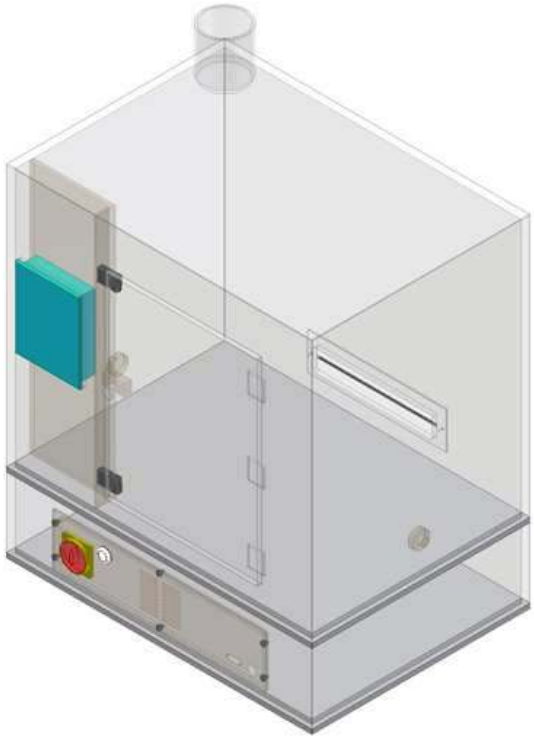

Figure 3.1: Drawing of the new electrospin cabin

(a)

(b)

Figure 3.2: The created electrospinning cabin. (a) Overview. (b) Operator Panel

3.3 Spiral spinner design

In the previous chapter the movement of the sheet above the grounded needle was initiated by hand. Because of the lack of accuracy in positioning and speed a motion controlled setup is needed to improve the possibilities to study the process in detail.
To investigate the influence of the collecting speed, the intermediate sheet will have to move via a speed controlled mechanism. To keep the setup as simple as possible the fiber should therefore be collected via a sort of rotating movement. Moving a thin sheet of material in a x-y space would require quite special and expensive equipment (fast linear x-y stage) which cannot be realized in a short time period and at low costs. An interim solution is to collect the fiber on a rotating drum or on a horizontal rotating disc.

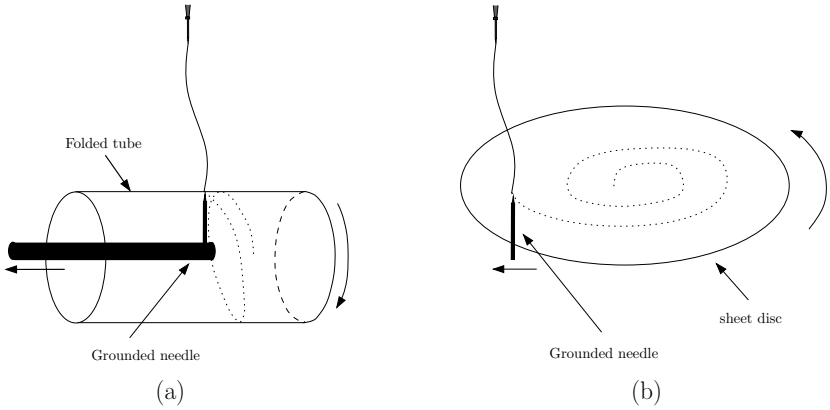

Figure 3.3: Sketchy interpretation of the interim solutions. (a) Collection on a rotating drum. (b) Collection on a rotating disc

The first method (Fig. 3.3 (a)) requires a tube of thin sheet material. Making these tubes requires quite a lot of labor and the unfolding after the experiment could also cause damage to the spun sample.
The second method (Fig. 3.3 (b)) only needs a disc which has been cut out of thin sheet material. After the experiment the disc is directly suited for examination and needs no further preparation (except for sputter coating, when used in a SEM). Because of these advantages the second method has been elaborated and a so called "spiral spinner" has been build.
The setup shows great similarity with a cd player mechanism. It contains a speed controlled rotating center-axis on which a disc of thin sheet material can be clamped, and a position controlled arm which holds and guides the grounded needle. A design sketch is shown in Fig. 3.4. The base plate and the arm are made out of (isolating) PVC and all metal parts are packed in PVC covers. The driving motors (servo's) are placed on the side of the setup with an isolating (PVC) screen in between. This is done to diminish the influence on the process because of the (electro magnetic) radiation from the motors. The arm and the disk are driven via small belts and cogwheels underneath the setup. In order to prevent charging of the setup via the rotating disc, the center-axis has been specially made out of the high insulating material *Celleron*.

(a)

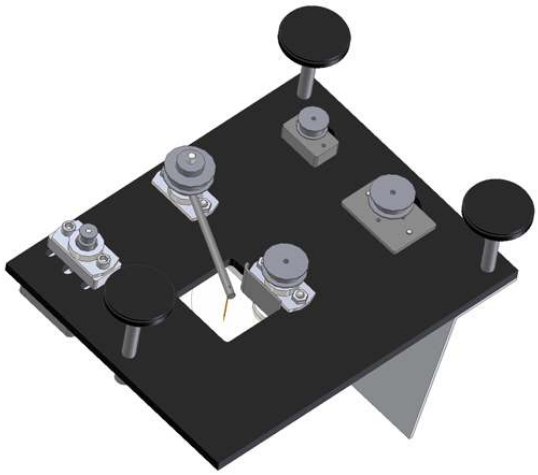

(b)

Figure 3.4: Design sketches of the spiral spinner. (a) isometric view. (b) bottom view.

The whole setup is controlled by Matlab Simulink via a TUeDACS AQI data acquisition unit [26]. The motor of the disc is equipped with a tachometer to measure the rotation speed and the arm is equipped with an incremental encoder to measure the angle of the arm. This encoder has been connected to the arm-axis via a smaller cogwheel in order to get an improved positioning resolution for the arm.
To make a long-term pickup of fiber possible the disc and the arm will follow the contour of an archimedean spiral (see Fig. 3.5). In polar coordinates (r, θ) this spiral can be described by the equation:

$$r = a + b\theta \tag{3.1}$$

with a the starting radius and b the distance between successive turnings. The

characteristic feature of this type of spiral is that successive turnings of the spiral have a constant separation distance equal to $2\pi b$. The control scheme should be setup in such a way that the speed of the disc is adapted, as the radius (position of the needle) is increased, to maintain a constant collecting speed over the whole disc.

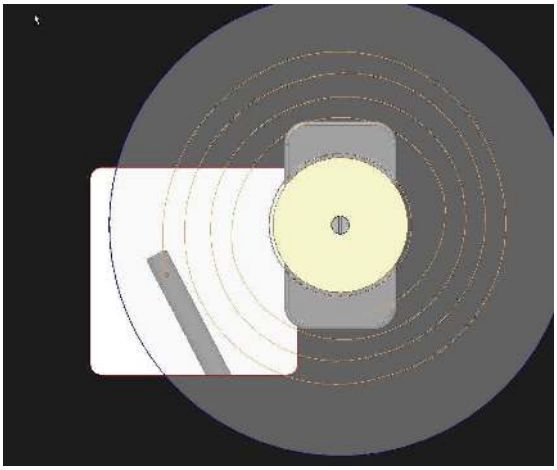

Figure 3.5: Sketch of a archimedean spiral on the disc in the setup.

To operate the setup a graphical user interface (GUI) has been made which operates the Simulink control file (see Fig. 3.6). Via this interface the setup can be initialized (setting the arm in the right starting angle) and the desired disc speed and the distance between the successive turnings can be set. In order to make the application of different disc-sizes possible, the travel angle of the arm can also be adapted.

Finally, the setup (see Fig. 3.7) has been identified by two FRF measurements and proper controllers have been derived via the loopshaping procedure [27, 28]. The remaining positioning error of the arm is approximately 0.15 degrees which corresponds to 0.25 mm positioning error at the tip of the grounded needle. The speed of the disc has a remaining error of approximately 0.2 m/s, for a typical value of 4 m/s. The achieved precision should, for the time being, be sufficient to investigate the focussing process more profoundly.
At last it should be noted that with this setup not only the sheet is moved, but also the grounded needle. It is believed that, although the approach is a little different from the method described in 2.4.2, the field can handle the relatively small and slow movement of the grounded needle. The limit to what extend this can be done before the process will get affected is, however, not known yet.

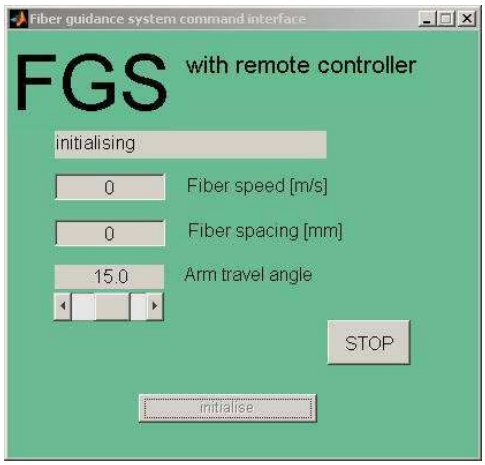

Figure 3.6: Graphical user interface

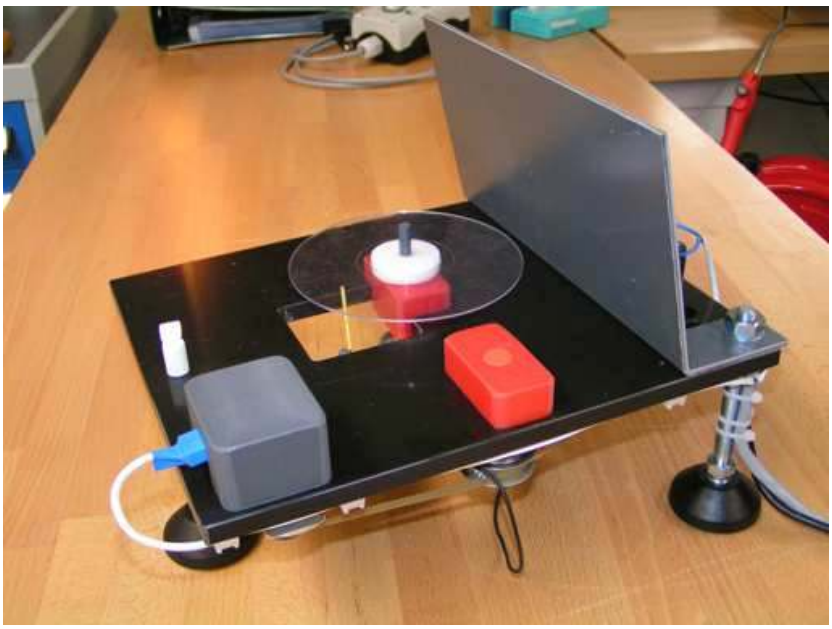

Figure 3.7: The 'spiral spinner' setup

4

Measurements & results

4.1 Introduction

In this chapter the use of the spiral spinner is described and the results are discussed. To give a better interpretation of these results, also a high speed camera is used to visualize the spinning process. The experimental details of using the high speed camera is elaborated with the accompanying results.

4.2 Spiral spinning

The first spiral spinning tests are performed using cd format (diameter $14cm$) mylar sheets, a distance between the tips of the needles of $7cm$ and an electric potential of $11kV$. The cabin is at room temperature (about $24°C$) and the polyethylene oxide solution is used as spinning material. The flow is set to $12\mu l/min$ in order to get a submicron fiber diameter.
At the start of each experiment, the infusion pump is started to form a small droplet at the tip of the blunt needle. A soon as the droplet is forming the disc is speeded up to the desired collecting speed. When the desired speed is reached and a small droplet is formed, the electric potential is powered up. As soon as the high voltage is present, the droplet starts to deform into a cone-like shape (taylor cone) and a jet is ejected. The jet goes through a sort of turn-on transient before it stabilizes and ultimately ejects uniformly at the tip.

4.2.1 Results

After the stable jet has been ejected from the nozzle it usually starts whipping a few centimeters below the ejection point. Near the deposit point above the disc it converges again and focusses towards the grounded needle location. Over the subsequent experiments the rotational speed of the disc has slowly been increased whereas the spiral distance has been kept constant at $1mm$. Fig. 4.1 shows the results of these experiments with rotational speeds ranging from $2 - 8m/s$. The pictures have been taken with a Zeiss lightmicroscope (type Axioplan 2) using a lens with 5x magnification.
The first figure (Fig. 4.1 (a)) already shows a great improvement in the collection-nature in comparison with Fig. 2.8. The entwinement into a porous

thread seems to slowly disappear when a higher rotational speed is applied. This observation now provides an opportunity to not only align an entwined fiber, but also to align one single fiber. By slowly increasing the collecting speed indeed a single fiber alignment is feasible, as can be concluded from Fig. 4.1 (d). The collected fiber is around $800nm$ in diameter.

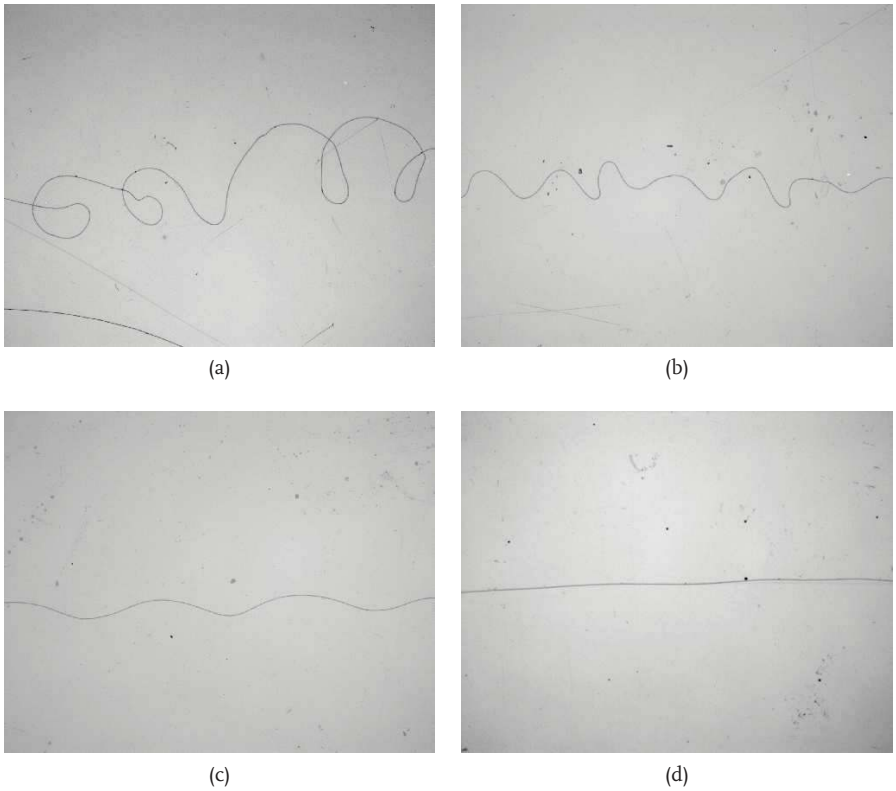

(a) (b)

(c) (d)

Figure 4.1: Microscopic images of electrospun spirals on a mylar disc with different collecting speeds. Collecting speeds: (a) $2m/s$ (b) $4m/s$ (c) $6m/s$ (d) $8m/s$. The height of each picture corresponds to approximately $0.5mm$

Another remarkable observation is the decreasing haze of whipping fiber between the needle tips, as the rotational speed is increased. This could mean that the whole instability in the fiber deposition can be faded out by using proper collecting speeds. The whipping fiber-instability is stretched out by the moving collection surface, which results in a straight fiber deposition.
A few papers report similar results [22, 29], however, the alignment of one fiber in a one dimensional 'large space' together with a stabilized deposition has not been reported yet!
The achieved results show much more potential than originally was anticipated for. Instead of controlling the deposition of an entwined porous thread now one single submicron fiber might even be positioned. To investigate the possible accuracy a much more precise motion controlled setup is required, because the accuracy of the setup is now coarse in comparison with the fiber diameter. Therefore a good distinction between the positioning error of the grounded needle and the depositing fiber cannot be made anymore.

Another problem is the onset of vibrating waves in the mylar disc at higher rotational speeds ($6 - 8m/s$). The mylar discs have been manually cut out by a self made cutting device. However the cut out looks fairly uniform it will not be perfectly round, and will therefore lead to little rotational instabilities.
Fig. 4.2 shows a comparison between two surfaces of a spun disc with a collecting speed of $2m/s$ and $8m/s$. Each picture has been taken with a Nikon digital camera (type D50 with a 105mm micro Nikkor lens). Fig. 4.2 (a) shows the collected fiber at $2m/s$. The spiral is quite uniform and shows no large deviations from the spiral form. Fig. 4.2 (b) shows the collected spiral at $8m/s$. Because of the little instabilities in the disc the spiral form now shows some deviations with amplitudes ranging over $0.25mm$.

(a) (b)

Figure 4.2: Surfaces of spun discs with different collecting speeds. Collecting speeds: (a) $2m/s$ (b) $8m/s$.

A way to prove that the vibration influences the fiber collection and that this is less caused by the setup accuracy, the diameter of the disc can be reduced because a reduction in diameter also should reduce the amount of vibrations in the rotating disc. To also be sure that a better uniform cutout is achieved the smaller disc (diameter $8cm$) has been cut on a turning machine using a press mould.
Figure 4.3 shows the result of the experiment using the smaller disc. Because of the smaller diameter, the distance between successive turnings has been reduced to a (desired) spacing of $0.25mm$ in order to spin a nice amount of turnings on the disc. The figure shows that the amplitude of the deviations has been reduced ($< 0.1mm$), so it can be concluded that the instability of the disc does influence the collection of the fiber. In the figure also the error in the needle position might be recognized (distance between different successive turnings).

4.3 High speed imaging

Because the above discussed results are not totally conclusive, a high speed video camera has been applied in order to visualize the electrospinning process in real time.

Figure 4.3: Electrospun spirals on a smaller mylar disc with a collecting speed of $8m/s$ and a (desired) spacing of $0.25mm$. The image has been taken on a Zeiss lightmicroscope (type Axioplan 2) using a lens with 2,5x magnification

Recording the spinning process is a difficult task. The process area above the disc encloses approximately 4 by 4 cm, while the collected fiber has a (sub)micron diameter. Because of the great difference in size, it is very difficult to make the fiber visible within the desired space. To get the fiber visible it has to be lighted out quite precisely. Two high power special video lamps (type Dedocool) are used to enlighten the setup on the front and along the side. This reflects just enough light from the setup towards the camera to make the desired part of the setup visible. A so called backlight (small microscope light) is used to directly shine into the lens from behind the setup. This backlight ensures the fiber to be visible in the form of a shadow. The camera which has been used is a *Phantom* $V9.0$ high speed digital camera from *Vision Research* [30]. This camera can record over one thousand images per second at full resolution of 1632×1200 pixels and up to over 150 thousand images at 96×8 pixels. Two coupled tele-converters between the camera and the lens (a micro Nikkor 55mm portrait lens) create a working distance of $300mm$ and so the disc area can be captured from outside the cabin. The illumination scheme and the camera are presented in Fig. 4.4.
Although the smaller mylar discs produce less vibrations, they are not suppressed enough to obtain good images with the camera. For the high speed imaging tests the mylar disc has therefore been exchanged by a thin glass disc ($0.55mm$ thick). This disc can be rotated at the desired velocities without significant vibrations. Because the glass disc is thicker than the mylar disc, the high voltage has been increased to $12.5kV$ to overcome the loss in fieldstrength because of the thicker intermediate insulating film and to make the fiber also better visible the flow has been increased to $18\mu l/min$ which results in a little increase in diameter. The big conical shaped needle has been exchanged by a small copper strand ($0.1mm$ in diameter) to overcome focussing problems with the bigger needle.
In order to be sure that the adapted process indeed produces nice uniform fibers without the deviations an experiment has been carried out using the glass disc. In Fig. 4.5 the result of this experiment is presented showing a nice uniform collection of slightly thicker fibers and indeed without any deviations.

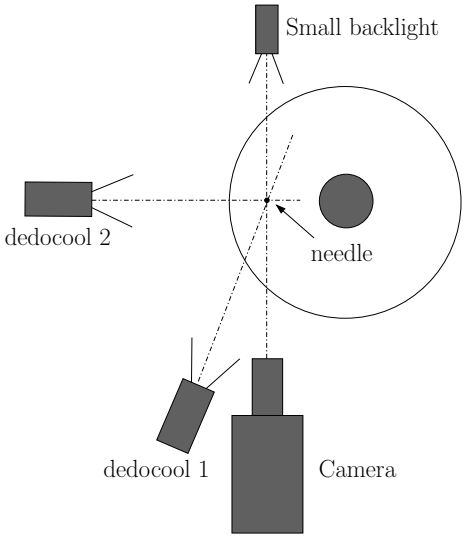

(a)

(b)

Figure 4.4: High speed camera utilization. (a) Lighting setup. (b) Highspeed camera with the 2x tele-converted portrait lens (55mm micro nikkor) and Dedocool video lamp.

4.3.1 Results

Several experiments have been performed at a rotational speed of $8m/s$ at different camera angles. The recorded images provide, although a little blurry, a successful view of the electrospinning process. Fig. 4.6 gives an impression of the front and side angles.

The images show the collection of one straight fiber, which means that the whipping instability indeed is faded out at higher collecting velocities. This again is quite a remarkable result, because other literature [22, 29, 31, 32, 33] does not report the collection of a fiber without the whipping instability.

The images also show that the fiber is bend into a curved shape. This is because as soon as the falling fiber reaches the disc, it is pulled away at the collecting speed

Figure 4.5: Electrospun spirals on a small glass disc with a collecting speed of $8m/s$ and a spacing of $1mm$. The image has been taken on a Zeiss lightmicroscope (type Axioplan 2) using a lens with 1,5x magnification

($8m/s$) resulting in a bended fiber. However, although the fiber now is aligned and stabilized, the pulling force induces a great positioning error. In Fig. 4.6 also a pixel measurement of this error compared to a known measure is sketched. The real pixel measurement has been made by the *'pixval'* tool of the *'image processing toolbox'* in *Matlab*.
The known measures are the thickness of the glass disc and the teflon lock ring, being $0.55mm$ and $3mm$ respectively. With a pixel width for the error in Fig. 4.6 (a) of 76 pixels and for Fig. 4.6 (b) of 327 pixels the recalculation gives a front-error of $1.75mm$ and side-error of $7.8mm$. It should be noted that this calculation is only based on one picture of two similar experiments at different angles. The whole movies of the two processes show a stable fiber position (error) during the whole experiment. The pictures which are presented here are based on the worst case findings.

It is believed that part of the error, measured on the front angle, can be explained by the pulling effect measured at the side angle. The side angle shows an error of approximately $8mm$. The curved fiber could still follow the spiral form explaining the measured front error. In Fig. 4.7 a sketch is presented in which the side error is plotted against the spiral form. By taking almost the same radial location in the figure as on the disc, the error of $7.8mm$ on the side resembles a deflection of approximately $1mm$ at the front. This might already explain almost 60% of the front measured error, but because the two pictures come from two different experiments again no conclusive answer about the errors can be derived. Another explanation for the front-angle error also could be the increasing vertical distance between the two needles while the arm is moving towards the rim of the disc. The movies indeed show a little increase in the front angle error, but on the other hand the spiral deflection also becomes larger as the spiral grows, leading to the same explanation.

The high speed imaging experimentation has visualized the electrospinning

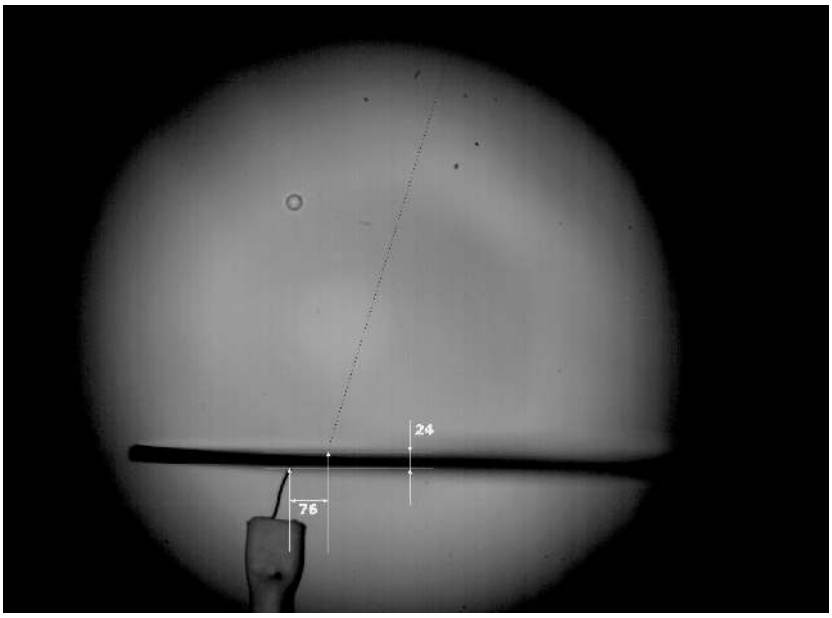

(a)

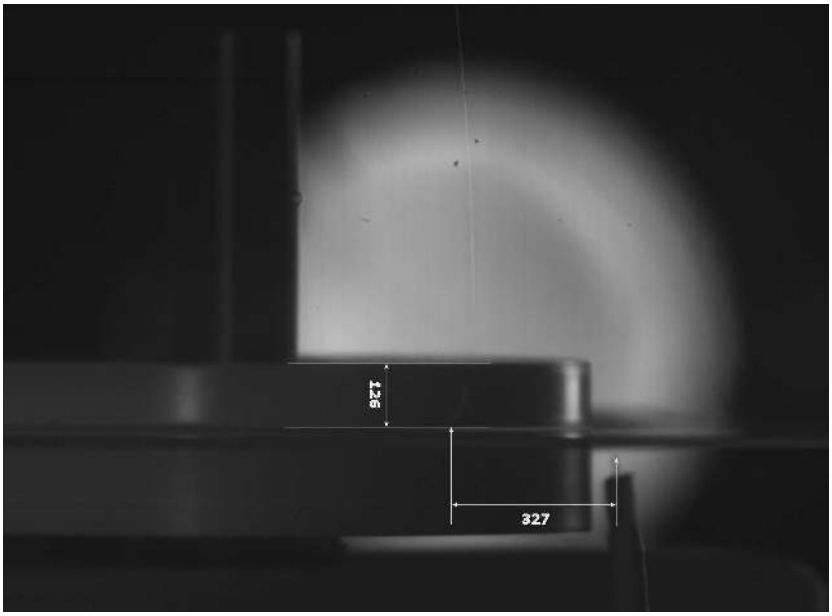

(b)

Figure 4.6: High speed imaging measurement results. (a) Pixel measurement of front view. (b) Pixel measurement of side view.

process with remarkable results. Because it was not possible to film two angles at once, a conclusive explanation for the present errors cannot be given yet.
Looking at the side-angle measurement it has become clear that the fiber is pulled away from the grounded needle by the rotation of the disc. It is believed that the

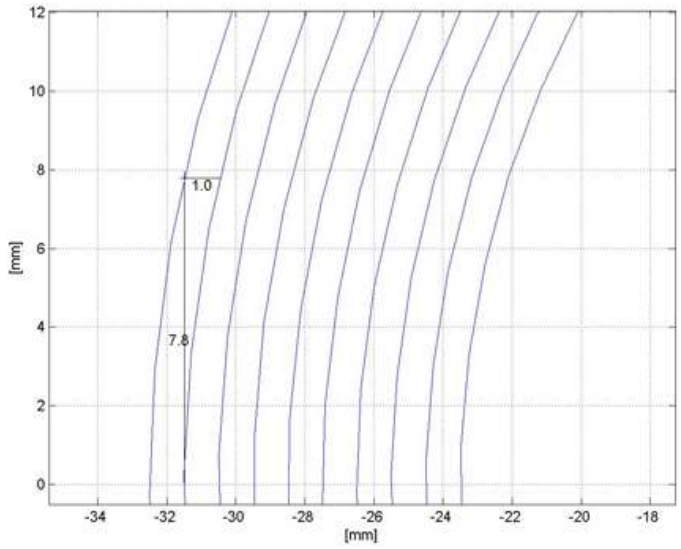

Figure 4.7: Top view of a spiral sketch with the experimental measures. The black lines represent the fiber deflection in mm

rotation of the disc also has an effect on the diameter of the fiber. The tangential force which pulls the fiber in an arc may also stretch the collecting fiber which results in a reduction of the fiber diameter.

5

Modeling the stretching of an electrified polymer jet

5.1 Introduction

In the previous chapter the bending of the fiber was demonstrated, caused by the rotational movement of the disc. A model description of this bending fase could help acquiring a better understanding of this process. In this chapter a sort of take-off point for a model based interpretation of this process is presented.
The paper of J. Feng [34] presents a model which describes the electrospinning process from the nozzle until the (whipping) instability point. This is the so called "first stage" of the process. During the disc-spinning process the jet is continuously winded up on the disc. The charge repulsion which normally generates the bending instability is therefore almost entirely cancelled out(the "second stage"). This model is therefore considered to be a good starting point. The model of J. Feng will be elaborated and tested by computer simulations. This model describes the radial reduction of the fiber diameter for newtonian polymer solutions.

5.2 Slender-body theory

The elongation of the jet during electrospinning is initiated by electrostatic force and gravity. Also inertia, viscosity and surface tension play an important role. The flow field and electric field are coupled, because during the thinning of the jet the surface charge density (σ) varies, which directly effects the electric field (E) and the pulling force.
The solution can be assumed to be weakly conducting and according to Saville [35]) the "leaky dielectric model" applies. This means that the jet carries electric charges only on its surface. Charges, present in the interior of the jet, are quickly conducted to the surface. At the same time the fluid is sufficiently dielectric so it is able to sustain an electric field tangential to the jet surface.

The slender-body approximation is according to [34] a familiar concept in modeling jets and drops. The standard assumptions for slender jets are: the jet radius R decreases slowly along the axial direction $z : |dR(z)/dz| \ll 1$ and the axial velocity v is uniform in the cross section of the jet. Now the flow is simplified to a nonuniform elongation, with all quantities depending only on the axial position z.

5.2.1 Equations

The jet can be represented by four steady-state equations: the conservation of mass and electric charges, the linear momentum balance and Coulomb's law for the E field.
Mass conservation can be stated by

$$\pi R^2 v = Q, \tag{5.1}$$

where Q is a constant volume flow rate. R is the jet radius and v is the constant axial fluid velocity within the jet. The current carried by the jet consists of charge conduction (within the jet) and charge convection (on the surface of the jet). The charge conservation can be stated by

$$\underbrace{\pi R^2 K E}_{conduction} + \underbrace{2\pi R v \sigma}_{convection} = I, \tag{5.2}$$

where I is the current carried by the jet,K is the electrical conductivity of the jet, E is the electric field strength and σ is the surface charge density.
The momentum equation is formulated by considering the forces on a short segment of the jet (see Fig. 5.1).

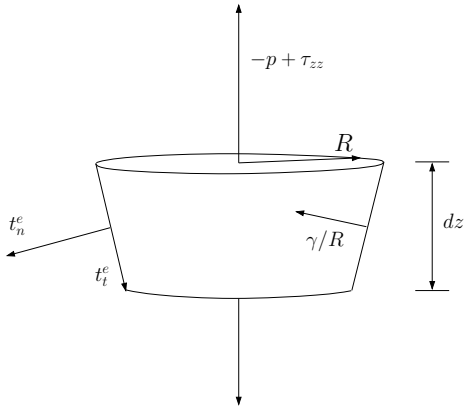

Figure 5.1: Momentum on a short jet-section

$$\frac{d}{dz}(\pi R^2 \rho v^2) = \pi R^2 \rho g + \frac{d}{dz}[\pi R^2(-p+\tau_{zz})] + \frac{\gamma}{R} \cdot 2\pi R R' + 2\pi R(t_t^e - t_n^e R'), \tag{5.3}$$

where τ_{zz} represents the viscous axial normal stress, p the pressure, γ the surface tension and t_t^e and t_n^e are the tangential and normal forces exerted on the jet by

the electric field. These terms can be derived with the help of the leaky electric model to be [35]

$$t_n^e \approx \frac{\sigma^2}{2\overline{\epsilon}} - \frac{\overline{\epsilon} - \epsilon}{2} E^2 \tag{5.4}$$

$$t_t^e \approx \sigma E \tag{5.5}$$

where ϵ and $\overline{\epsilon}$ are respectively the dielectric constants of the jet and the ambient air. The pressure $p(z)$ can be determined by the momentum balance in radial direction

$$-p + \tau_{rr} = t_n^e - \frac{\gamma}{R}. \tag{5.6}$$

Inserting Eqs. (4)-(6) into Eq. (3) gives the final momentum equation

$$\rho v v' = \rho g + \frac{3}{R^2}\frac{d}{dz}(\eta R^2 v') + \frac{\gamma R'}{R^2} + \frac{\sigma\sigma'}{\overline{\epsilon}} + (\epsilon - \overline{\epsilon})EE' + \frac{2\sigma E}{R}, \tag{5.7}$$

Hereby, for the time being, a generalized Newtonian constitutive relation has been used for the viscous normal stress difference:

$$\tau_{zz} - \tau_{rr} = 3\eta v'. \tag{5.8}$$

The viscosity η may depend on the local strain rate. The equation for the potential along the centerline of the jet can be derived from Coulomb's law:

$$\phi(z) = \phi_\infty(z) + \frac{1}{2\overline{\epsilon}} \int \frac{\sigma R d\zeta}{\sqrt{(z-\zeta)^2 + R^2}} - \frac{\beta}{4} \int \frac{d(ER^2)/d\zeta}{\sqrt{(z-\zeta)^2 + R^2}} d\zeta, \tag{5.9}$$

where $\beta = \epsilon/\overline{\epsilon} - 1$, and ϕ_∞ is the potential due to the external electric field. In [34] an asymptotic approximation is used to evaluate the integrals mentioned above. This leads to the final relation for the axial electric field:

$$E(z) = E_\infty(z) - ln\chi\Big(\frac{1}{\overline{\epsilon}}\frac{d(\sigma R)}{dz} - \frac{\beta}{2}\frac{d^2(ER^2)}{dz^2}\Big), \tag{5.10}$$

where $\chi = L/R_0$ with L the length of the gap between the nozzle and deposition point and R_0 the initial jet radius.
Now we have Eqs. (1), (2), (7), and (10) for the four unknown functions R, v, E and σ.

5.2.2 Scaling

According to [34] the parameters can be arranged into three categories: process parameters (Q, I and E_∞), geometric parameters (R_0 and L) and material parameters (ρ, η_0, ϵ, $\overline{\epsilon}$, K, and γ). Hereby is R_0 the radius at the origin of the jet just outside the nozzle, and η_0 is the zero-shear-rate viscosity.
The equations can be converted to dimensionless form using the following characteristic scales and dimensionless groups:

Characteristic scales:

$$\begin{aligned} \text{Length:} \quad & R_0, \\ \text{velocity:} \quad & v_0 = \frac{Q}{\pi R_0^2}, \\ \text{electric field:} \quad & E_0 = \frac{I}{\pi R_0^2 K}, \\ \text{surface charge density:} \quad & \sigma_0 = \overline{\epsilon} E_0 \end{aligned}$$

Dimensionless groups:

$$\begin{aligned} \text{Electric Peclet number:} \quad & Pe = \frac{2\overline{\epsilon} v_0}{K R_0}, \\ \text{Froude number:} \quad & Fr = \frac{v_0^2}{g R_0}, \\ \text{Reynolds number:} \quad & Re = \frac{\rho v_0 R_0}{\eta_0}, \\ \text{Weber number:} \quad & We = \frac{\rho v_0^2 R_0}{\gamma}, \\ \text{aspect ratio:} \quad & \chi = \frac{L}{R_0}, \\ \text{Electrostatic force parameter:} \quad & \varepsilon = \frac{\overline{\epsilon} E_0^2}{\rho v_0^2}, \\ \text{Dielectric constant ratio:} \quad & \beta = \frac{\epsilon}{\overline{\epsilon}} - 1 \end{aligned}$$

Inserting these dimensionless groups into Eqs. (1), (2), (7) and (10) gives the following dimensionless equations (the accents to indicate the dimensionless equations are left out for convenience):

$$R^2 v = 1, \tag{5.11}$$

$$ER^2 + PeRv\sigma = 1, \tag{5.12}$$

$$vv' = \frac{1}{Fr} + \frac{3}{Re}\frac{1}{R^2}\frac{d(\eta R^2 v')}{dz} + \frac{1}{We}\frac{R'}{R^2} + \varepsilon\Big(\sigma\sigma' + \beta EE' + \frac{2E\sigma}{R}\Big), \tag{5.13}$$

$$E = E_\infty - ln\chi\Big(\frac{d(\sigma R)}{dz} - \frac{\beta}{2}\frac{d^2(ER^2)}{dz^2}\Big). \tag{5.14}$$

The current I is taken to be an independent parameter. In reality this parameter depends on several factors (including setup-details) in ways that are not fully understood. During validation, measured values will be used for I. The spinning cabin has been equipped with a current probe for measuring the process currents.

5.2.3 Boundary conditions

To formulate the boundary conditions we need to reformulate the continuity and charge conservation relationships (Eqs. (11) and (12)), σ, σ' and v, v' can be expressed in terms of R and E:

$$v = 1/R^2, \quad v' = -2R'/R^3, \tag{5.15}$$

$$\sigma = (1 - ER^2)R/Pe, \quad \sigma' = 1/Pe\Big((1 - 3ER^2)R' - E'R^3\Big). \tag{5.16}$$

Now the momentum- and E-field equations can be recast into two second-order ordinary differential equations for R and E, each requiring two boundary conditions. At the origin of the jet ($z = 0$) an obvious condition is (see also Fig. 5.2)

$$R(0) = 1. \tag{5.17}$$

At the deposit point (just above it!) asymptotic thinning conditions apply [36]. R and σ drop to zero and E approaches E_∞. The stretching of the jet is managed by a balance of inertia, gravity and tangential electrostatic force. The asymptotic scaling can be stated as $R(z) \propto z^{-1/4}$ and the following conditions at the deposit point ($z = \chi$) can be adopted.

$$R(\chi) + 4zR'(\chi) = 0, \tag{5.18}$$

$$E(\chi) = E_\infty. \tag{5.19}$$

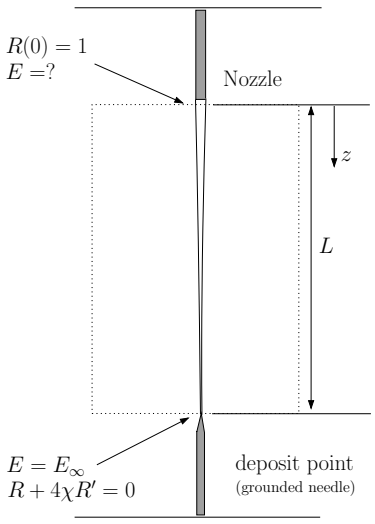

Figure 5.2: Boundary conditions

The last boundary condition concerns the surface charge density at the entrance σ_0. This parameter determines $E(0)$ for any given I through charge conservation. In the jet just underneath the nozzle, the charge has not had time to migrate to

the surface of the jet. In [34] it is widely discussed that a reasonable boundary condition to take is

$$\sigma(0) = 0. \tag{5.20}$$

In [34] this condition has been widely examined and the outcome is that the initial condition, derived for σ, only influences a tiny boundary layer region close to the nozzle. By using different initial conditions for σ it has been proven that the solutions converge to the same result.

5.3 Numerical solution of the model

The momentum and electric field equations can be rewritten into a set of four coupled first order ODE's with the above mentioned boundary conditions. This gives a boundary value problem, which can best be solved by a numerical relaxation method as e.g. $solvde$ from Numerical Recipes [37]. Other routines as e.g. shooting or collocation are unsuitable for solving this problem because the jacobians easily turn singular for certain initial guesses as starting values. Within relaxation methods [37] the differential equations are replaced by finite-difference equations on a certain mesh of points covering the range of integration. During iteration (relaxation) all the values on the mesh are adjusted to bring them into closer agreement with the finite-difference equations and the boundary conditions. For some problems relaxation works better than other methods, especially when the solutions are smooth and not highly oscillatory. The secret for efficient relaxation is providing good initial guesses. One often has to solve a problem many times, each time with a slightly different initial value of some parameter(s). In that case the previous solution will usually be a good initial guess after changing a parameter, and relaxation will work surprisingly fast.
The first step is to write the ODE's as a system of first order ODE's. The basic idea is to introduce new variables, one for each variable in the original problem and one for each of its derivatives up to one less than the highest derivative appearing.

5.3.1 rewriting the equations

The first step is to write the the equations as a system of first order ODE's. Substituting Eqs. (15) and (16) into (13) and (14) gives:

$$\frac{-2R'}{R^5} = \frac{1}{Fr} + \frac{3}{ReR^2}\frac{d}{dz}\Big(\frac{-2\eta R'}{R}\Big) + \frac{1}{We}\frac{R'}{R^2} + \varepsilon\Big(\sigma\sigma' + \beta EE' + \frac{2E(1-ER^2)}{Pe}\Big), \tag{5.21}$$

with

$$\sigma\sigma' = \frac{1}{Pe^2}(R - ER^3)\Big((1-3ER^2)R' - E'R^3\Big), \tag{5.22}$$

and

$$E = E_\infty - ln(\chi)\Big(\frac{d}{dz}\big(\frac{(1-ER^2)R^2}{Pe}\big) - \frac{\beta}{2}\frac{d^2(ER^2)}{dz^2}\Big). \tag{5.23}$$

Now by using the following states ($y_1 = R, y_2 = ER^2, y_3 = R', y_4 = (ER^2)'$) the first order equations can be derived:

$$y'_1 = y_3, \tag{5.24}$$

$$y'_2 = y_4, \tag{5.25}$$

$$\begin{aligned} y'_3 = \frac{Re}{6\eta}\Big(&\frac{2y_3}{y_1^2} + \frac{y_1 y_3}{We} + \frac{6\eta y_3^2}{Re y_1} - \frac{6\dot{\eta} y_3}{Re} + \frac{y_1^3}{Fr} + \frac{\beta\varepsilon y_2}{y_1^2}(y_1 y_4 - 2y_2 y_3) \\ &+ \frac{\varepsilon}{Pe^2} y_1^4 (1-y_2)(y_3 - y_1 y_4 - y_2 y_3) + \frac{2\varepsilon}{Pe} y_1 y_2 (1-y_2)\Big), \end{aligned} \tag{5.26}$$

$$y'_4 = \frac{2}{\beta}\Big(\frac{1}{ln(\chi)}\Big(\frac{y_2}{y_1^2} - E_\infty\Big) + \frac{1}{Pe}(2y_1 y_3 - y_1^2 y_4 - 2y_1 y_2 y_3)\Big). \tag{5.27}$$

The interpretation of the relaxation method and the implementation of the model into the relaxation routine can be found in appendix B.

5.4 Simulation experiments

The in appendix B implemented model has been converted into a FORTRAN main file which communicates with the **solvde** routine from Numerical recipes. To validate the solutions between the model in [34] and the model derived above, the same parameters for a Glycerol jet are used [34]:

$$\begin{aligned} R_0 &= 0.0008 \quad \text{m} \\ L &= 0.06 \quad \text{m} \\ Q &= 1/60 \times 10^{-6} \quad \text{m}^3/\text{s} \\ E_\infty &= 500 \quad \text{kV/m} \\ I &= 170 \quad \text{nA} \\ \nu &= 1.49 \times 10^{-3} \quad \text{m}^2/\text{s} \\ K &= 1 \times 10^{-6} \quad \text{S/m} \\ \gamma &= 6.34 \times 10^{-2} \quad \text{N/m} \\ \rho &= 1.26 \times 10^{3} \quad \text{kg/m}^3 \\ \overline{\epsilon} &= 8.854 \times 10^{-12} \quad \text{C}^2/\text{Nm}^2 \\ \epsilon/\overline{\epsilon} &= 46.5 \end{aligned}$$

Now the dimensionless parameters are:

$$\begin{aligned} \chi &= 75 \\ \beta &= 45.5 \\ Re &= 4.451 \times 10^{-3} \\ We &= 1.099 \times 10^{-3} \\ Fr &= 8.755 \times 10^{-3} \\ Pe &= 1.835 \times 10^{-4} \\ \varepsilon &= 0.7311 \\ E_\infty &= 5.914 \end{aligned}$$

With the above mentioned boundary conditions:

$$\begin{bmatrix} y_1(0) = 1 \\ y_2(0) = E(0) * y_1(0)^2 = E(0) \\ y_2(\chi) = E_\infty * y_1(\chi)^2 \\ y_1(\chi) + 4\chi y_3(\chi) = 0 \end{bmatrix}$$

The inlet boundary condition $E(0)$ can be calculated using $E(0) = 1 - Pe * \sigma(0)$. $E(0)$ has to be very close to 1 because $\sigma(0)$ normally is not that large. This calculation is necessary in order to simulate the small Pe numbers. Because a newtonian fluid is assumed the value for η should be taken 1.0 and of course this gives for $\dot{\eta} = 0.0$.
For moderately large χ convergence mostly fails. This can be helped by two methods. The first method is to use under-relaxation, this means that only a fraction of the full relaxation step will be used for the next step. This reduction helps convergence and can be controlled by the **slowc** parameter in the **fortran** program.
The second method is providing better initial guesses. Probably the best way to work towards larger values for χ is to start with a converged solution for small χ. Through personal contact with Mr. Feng a solution for $\chi = 20$ which has been obtained using some model testparameters has been provided (see Fig. 5.3). Next this solution can be interpolated and stretched to larger χ values. Nevertheless the parameters should be adjusted in such a way that they also meet the new exit conditions.

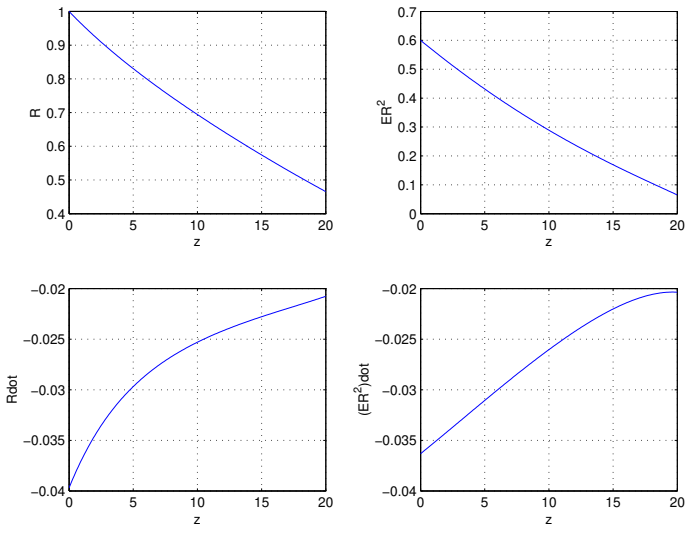

Figure 5.3: Converged solution for $\chi = 20$ calculated by J. Feng with testparameters

To obtain a converged solution for the above mentioned values the modelparameters have to be adapted through several steps, always using the converged solution as initial guess for the next step. The Pe number has turned out to be very sensitive for alteration, and for the model to preserve convergence

this parameter must be changed very slightly. The first step is stretching χ to 75 and altering the other parameters, except the Pe number, to the desired value. During the relaxation procedure the solution of Fig. 5.3 is stretched and interpolated to meet the new desired conditions. Now by using the solution of each step as initial guess for the next (without stretching or interpolation) and by modifying the Pe number using very small steps the model finally converges to the desired solution as showed in Fig. 5.4 and 5.5. This solution is almost exactly the same as solution (a) in Fig. 3 of [34].
By changing the RE number into $Re = 5.608 \times 10^{-3}$ and using the above obtained solution as initial guess, solution (b) in [34] also can be reproduced. See Fig. 5.6 and 5.7. Now by zooming into the range $0 \leq \chi \leq 5$ a better view of the dimensionless thinning radius is obtained. See Fig. 5.8. The curves are labeled with the same character as used in [34].

5.5 Concluding remarks

The model proposed by J. Feng has been elaborated and converted into a relaxation routine. With the help of a good initial guess a similar numerical result as in the paper has been obtained. Subsequently, this model was expanded to meet the actually used visco-elastic spinning materials [38].
The remarkable result of this model evaluation is that the extensive fiber thinning occurs within the first few millimeters under the nozzle. The rest of the gap towards the deposition point only functions as evaporation space to 'dry' the fiber. This observation gives rise to the idea of altering the setup of the process. If this large gap could be reduced, the observed bending of the fiber would also be reduced resulting in a much smaller position error.
The results obtained can also be used as a basis for creating a 2D spinning model for the prediction of the fiber bending on a moving deposition target. Together with an improvement of the spinning setup (reduction of the large gap) a good solution for the reduction of the deposition error might be developed.

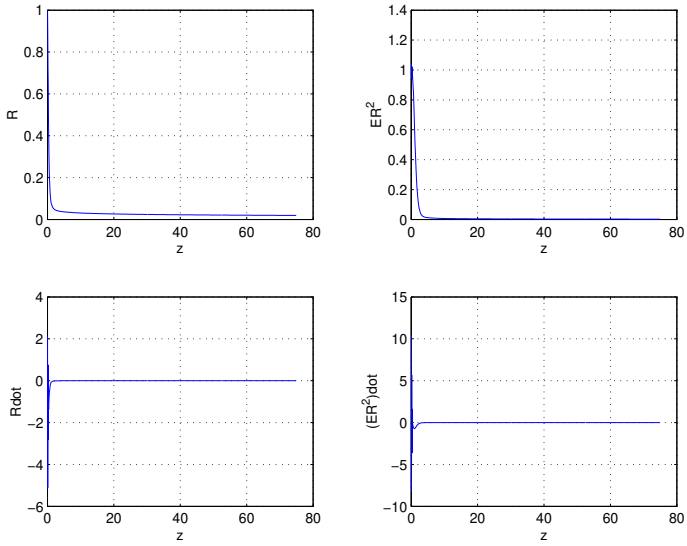

Figure 5.4: Converged solution for the glycerol parameters as mentioned in [34]

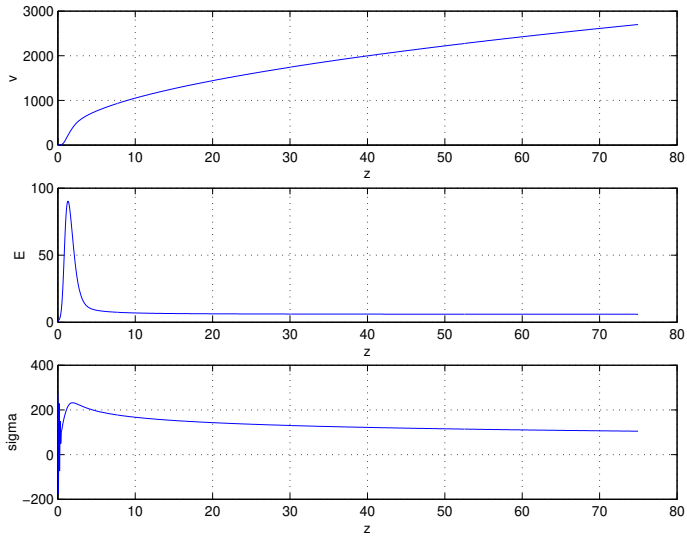

Figure 5.5: Accompanying results for v, E, σ for the glycerol jet

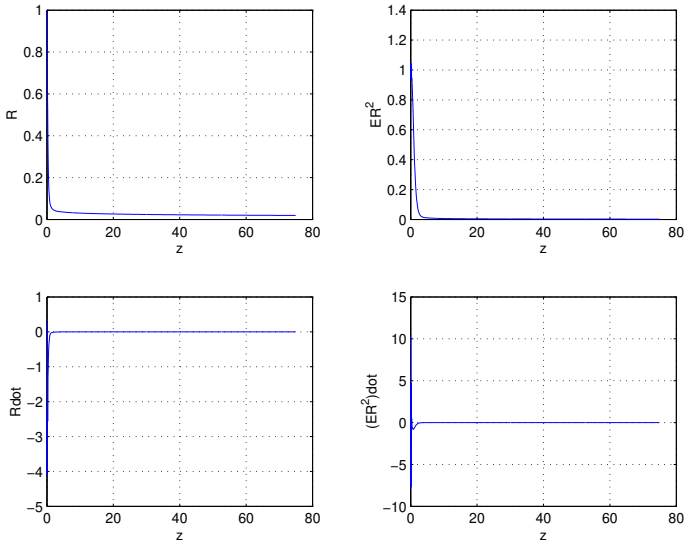

Figure 5.6: Converged solution for the glycerol parameters, only with slightly higher $Re = 5.608 \times 10^{-3}$

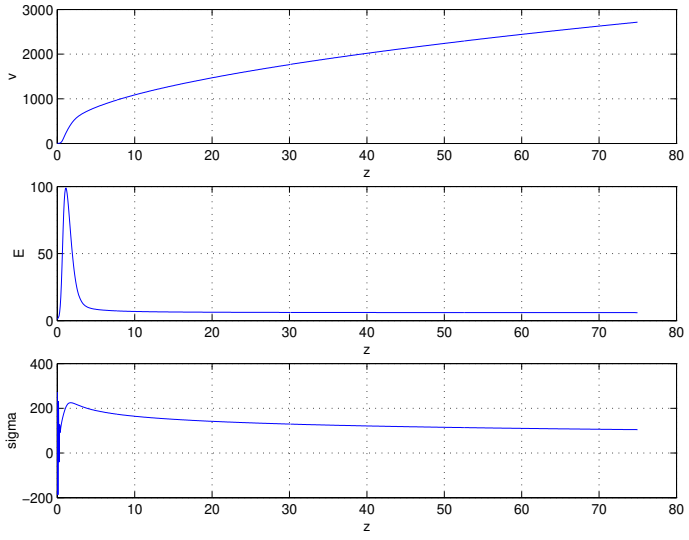

Figure 5.7: Accompanying results for v, E, σ for the adapted glycerol jet

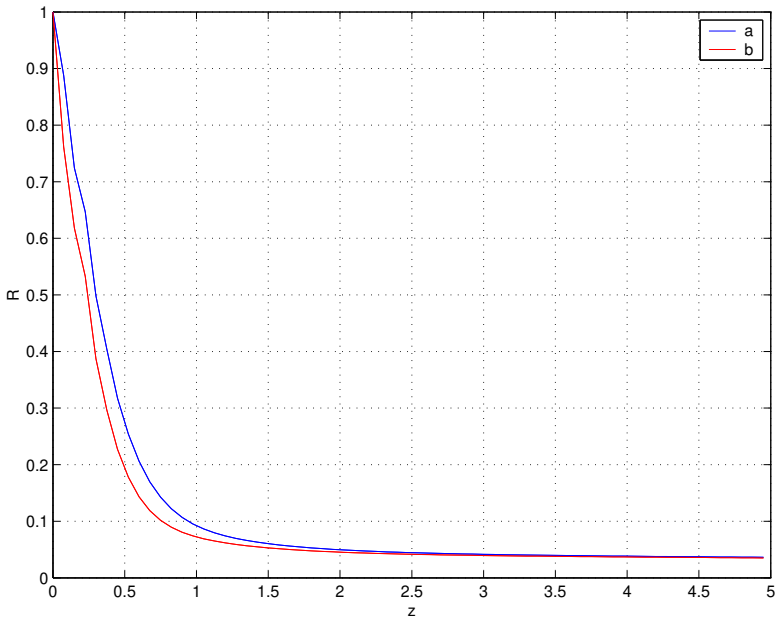

Figure 5.8: Zoom of the solutions of the derived model, (a) solution using the parameters as stated in [34], (b) solution using slightly higher $Re = 5.608 \times 10^{-3}$

6

Conclusions & Future work

6.1 Conclusions

The electrospin process has been investigated to identify the most important process parameters. Different usable spinning and deposition materials have also been investigated. To gain insight in the modification of the Electric field by the implementation of the grounded needle a FEM analysis has been carried out. This analysis has indicated that by using a grounded needle instead of a grounded plate the electric field indeed focusses towards the tip of the needle. To obtain physical proof an experimental test setup has been created and verification tests have been carried out. These tests have proven that focussing of the deposition really does occur. By also moving the deposition target it turned out to be possible to spin a nicely entwined uniform porous thread. This result has indicated that the focussing process on a grounded needle can become rather accurate and has much potential.
To investigate the focussing process more profoundly, specialized test equipment has been developed. This comprises the design of an electrospin cabin, which has been fully CE certified, and the design of a spiral spinner. The spinner is a plain motion controlled setup for the investigation of the influence of the collecting speed on the focussing process. Measurements with these developed instruments have shown that the focussing is dependent on the collecting speed. When a higher rotational speed is applied the entwinement into a porous thread slowly starts to disappear and at some point it even turned out to be possible to align one single fiber. An accompanying remarkable observation is the stabilization of the fiber ejection at higher collecting speeds.
A high speed video camera has been applied to visualize the electrospinning process. The recorded images show the collection of one straight fiber which proves the stabilization of the ejection. The images also show that the fiber is bend into an arc which causes a large positioning error in relation to the grounded needle. A few reasons for the error can be indicated, but a conclusive explanation for the error cannot be given jet.
A model description of this bending fase might help acquiring a better understanding of this occurrence. Therefore a starting point for a model based

interpretation of this process has been presented. The model, which describes the radial reduction of the fiber diameter for newtonian polymer solutions, has been elaborated and tested by numerical simulations. The remarkable result which has come out of this evaluation is that the extensive fiber thinning occurs within the first few millimeters under the nozzle. The rest of the gap towards the deposition point only functions as evaporation space to 'dry' the fiber.

6.2 Future work

In the previous chapter a starting point for a model based interpretation of the electrospinning process has been presented. It has also been indicated that a positioning error occurs through the high collecting speed of the disc. This error could be reduced by miniaturizing the process, and could also be compensated for by the use of an error prediction model. This model could predict the amount of bending of the fiber and this effect could then be attenuated by the control system. If the gap between the two needles could become much smaller, maybe a few millimeters, the resulting "pulling error" would also become much smaller. To still overcome the remaining error, a process model could predict the residual error and the motion controlled position could be adapted to compensate this.
To continue this research a few interesting directions can be extracted. First, the process could be miniaturized. This comprises the development of a small nozzle, an accurate needle positioning system and an accurate motion controlled carrier (x-y stage) for positioning the intermediate deposit materials between the two needles. A small nozzle should initiate a very small (taylor)cone-shaped ejection which should make a rather short fiber forming process possible. This eventually would lead to a large decrease of the essential gap distance between to two needles and an accurate positioning of these needles (gap distance) is therefore desired. A dedicated x-y stage should than make a one-dimensional fiber deposition possible with reduced positioning error (dependent on the amount of miniaturization this stage should have a traveling speed of $1m/s$ down to 20 cm/s with a positioning accuracy of $\approx 1\mu m$ and a stroke of approximately $50 \times 50mm$).
Second, the evaluated model should be further elaborated towards the use of visco-elastic solutions, Since the materials which are being used for spinning are visco-elastic in behaviour. TU/e student Peter Roozemond [38] has already been working on the elaboration of such a model. With the outcome of this study a real process model (in 2D or 3D) could be developed to predict the bending of the fiber into an arc above a moving deposition target.
The presented technique shows very much potential which, with the proper research, could finally lead to new pioneering spinning machines which are able to make woven fabrics or straight single fibers with micron-scaled resolutions. Therefore a search for interested cooperation partners or investors will be initiated. The whole research will also be converted into a business idea which will join the STW 'orientation for entrepreneurship' challenge to get an idea of the amount of interest from the industry.
At the time that this report was written a paper [39] from the University of California, Berkely, was published. The authors present a Near Field Electrospinning method which comprises the miniaturization of the electrospinning process. Although their approach is a little different it truly confirms the potential of the above elaborated idea.

Bibliography

[1] A. Formhals. Us patent, 1,975,504, (1934).

[2] A. Formhals. Us patent, 2,160,962, (1939).

[3] A. Formhals. Us patent, 2,187,306, (1940).

[4] A. Formhals. Us patent, 2,323,025, (1943).

[5] A. Formhals. Us patent, 2,349,950, (1944).

[6] Donaldson filtration solutions. Ultra-web nanofiber filter media. company website: www.donaldson.com/en/filtermedia/index.html.

[7] Phillip Gibson, Heidi Schreuder-Gibson, and Donald Rivin. Transport properties of porous membranes based on electrospun nanofibers. *Colloids and Surfaces A*, 187-188:469–481, 2001.

[8] Darrell H. Reneker Jong-sang Kim. Mechanical properties of composites using ultrafine electrospun fibers. *Polymer composites*, 20(issue 1):124–131, 2004.

[9] van Lieshout M.I., Vaz C.M., Rutten M.C., Peters G.W.M., and Baaijens F.P.T. Electrospinning versus knitting: two scaffolds for tissue engineering of the aortic valve. Technical Report 164111600, TU/e, 2006.

[10] Byung-Moo Min, Gene Lee, So Hyun Kim, Young Sik Nam, Taek Seung Lee, and Won Ho Park. Electrospinning of silk fibroin nanofibers and its effect on the adhesion and spreading of normal human keratinocytes and fibroblasts in vitro. *Biomaterials*, 25(7-8):1289–1297, 2004.

[11] Vaz C.M., van Tuijl S., Bouten C.V., and Baaijens F.P.T. Design of scaffolds for blood vessel tissue engineering using a multi-layering electrospinning technique. Technical Report 16701837, TU/e, 2005.

[12] Andrea Townsend-Nicholson and Suwan N. Jayasinghe. Cell electrospinning: a unique biotechnique for encapsulating living organisms for generating active biological microthreads/scaffolds. *Biomacromolecules*, 7(12):3364–3369, 2006.

[13] N. J. Pinto, Jr. A. T. Johnson, A. G. MacDiarmid, C. H. Mueller, D. C. Robinson N. Theofylaktos, and F. A. Miranda. Electrospun polyaniline/polyethylene oxide nanofiber field-effect transistor. *Applied Physics Letters*, 83(20):4244–4246, 2003.

[14] Haiqing Liu, Jun Kameoka, David A. Czaplewski, and H. G. Craighead. Polymeric nanowire chemical sensor. *Nano Letters*, 4:671 –675, 2004.

[15] Xianyan Wang, Christopher Drew, Soo-Hyoung Lee, Kris J. Senecal, Jayant Kumar, and Lynne A. Samuelson. Electrospun nanofibrous membranes for highly sensitive optical sensors. *Nano Letters*, 2:1273 –1275, 2002.

[16] M Kotaki S. Ramakrishna Zheng-Ming Huang, Y.-Z. Zhang. A review on polymer nanofibers by electrospinning and their applications in nanocomposites. *Composites Science and Technology*, 63:2223–2253, 2003.

[17] Dan Li and Younan Xia. Electrospinning of nanofibers: Reinventing the wheel? *Advanced Materials*, 16(14):1151, 2004.

[18] Y.M. Shin, M.M. Hohman, M.P. Brenner, and G.C. Rutledge. Experimental characterization of electrospinning: the electrically forced jet and instabilities. *Polymer*, 42:9955–9967, 2001.

[19] G.W.M. Peters & M.J.G. vd. Molengraft. Werkwijze en inrichting voor het met behulp van een electrisch veld uit een materiaal vervaardigen en sturen van een vezel, en voorwerp aldus vervaardigd. patent no. 1028847, Technische universiteit Eindhoven, 2005.

[20] Royal Kessick, John Fenn, and Gary Tepper. The use of ac potentials in electrospraying and electrospinning processes. *Polymer*, 45:2981–2984, 2004.

[21] G. I. Taylor. Proc. roy. soc. london,a313,453, (1969).

[22] A. Theron, E. Zussman, and A.L. Yarin. Electrostatic field-assisted alignment of electrospun nanofibres. *Nanotechnology*, 12:384–390, 2001.

[23] Garth Wilkes. Electrospinning. introduction website with experimental results, available from website: *http://www.che.vt.edu/Wilkes/electrospinning/electrspinning.html*.

[24] H. Fong, I. Chun, and D. H. Reneker. Beaded nanofibers formed during electrospinning. *Polymer*, 40(16):4585, 1999.

[25] Comsol (Femlab GmbH). Finite element modeling analysis programm. company website: http://www.femlab.de/products/acdc/.

[26] Bedrijfsgroep Laboratorium automatisering (BLN). Tuedacs aqi data acquisition unit. websites: http://www.dct.tue.nl/wintarget01.htm and http://www.tuedacs.nl/Products/AQI/AQI.html.

[27] Johan Boot. Frequency response measurement in closed loop: brushing up our knowledge. Technical report, University of Technology Eindhoven, 2003.

[28] M. Steinbuch. Coursenotes digital motion control, 2003.

[29] Jun Kameoka, Reid Orth, Yanou Yang, David Czaplewski, Robert Mathers, Geoffrey W Coates, and H G Craighead. A scanning tip electrospinning source for deposition of oriented nanofibres. *Nanotechnology*, 14:1124–1129, 2003.

[30] Vision research. Phantom high-speed imaging. camera version 9.0. company website: http://www.visionresearch.com.

[31] Jun Kameoka and H. G. Craighead. Fabrication of oriented polymeric nanofibers on planar surfaces by electrospinning. *Applied Physics Letters*, 83(2):371–373, 2003.

[32] J.M. Deitzel, J.D. Kleinmeyer, J.K. Hirvonen, and N.C. Beck Tan. Controlled deposition of electrospun poly(ethylene oxide) fibers. *Polymer*, 42:8163–8170, 2001.

[33] Dan Li, Yuliang Wang, and Younan Xia. Electrospinning nanofibers as uniaxially aligned arrays and layer-by-layer stacked films. *Advanced Materials*, 16(4):361, 2004.

[34] J.J. Feng. The stetching of an electrified non-newtonian jet: A model for electrospinning. *Phys. Fluids*, 14(11), 2002.

[35] D.A. Saville. Electrohydrodynamics: The taylor-melcher leaky dielectric model. *Fluid Mech*, 29(27), 1997.

[36] V.N.Kirichenko, I.V.Petryanov-Sokolov, N.N Suprun, and A.A. Shutov. Asymptotic radius of a slightly conducting liquid jet in an electric field. *Sov. Phys.*, 31(611), 1986.

[37] William H. Press, Saul A. Teukolsky, William T. Vetterling, and et al. *Numerical recipes in Fortran 90, the art of parallel scientific computing*. 1996.

[38] P.C. Roozemond. A model for electrospinning viscoelastic fluid. Bachelor Final Project 0576690, TU/e, 2007.

[39] Daoheng Sun, Chieh Chang, Sha Li, and Liwei Lin. Near-field electrospinning. *Nano Letters*, 6(4):839–842, 2006.

A

Gebruikershandleiding E-spin Cabine

Apparaat:

E-spincabine
Bouwjaar 2007
CE IIA

Project nr.: 10005484
Versie: 1.0

Fabrikant:

Faculteit Werktuigbouwkunde &
Gemeenschappelijke Technische Dienst
Technische Universiteit Eindhoven
Den Dolech 2 Postbus 513
5612 AZ Eindhoven 5600 MB Eindhoven

A.1 Gebruik

A.1.1 Beoogd gebruik

De E-spincabine is bedoeld voor het gebruik in een laboratorium door ter zake kundig personeel, met als doel het spinnen van polymeer oplossingen met behulp van een electrostatisch veld. Dit veld wordt opgewekt door een hoogspanning tussen 2 punten aan te brengen. Het toegepaste voltage bij deze opstelling reikt tot 25 kV!

A.1.2 Ontraden gebruik

De cabine is niet geschikt voor experimenten met hoogspanning anders dan het spinnen van dunne vezels!

De cabine wordt bedreven met een zeer hoog voltage. De lopende stroom door de opstelling kan hierbij reiken tot $1\mu A$***. Deze waarden zijn in staat het menselijke hartritme te ontregelen. De veiligheidsaspecten dienen dan ook te allen tijde in acht te worden genomen! Enig contact met de hoogspanning dient te worden vermeden in verband met levensgevaar!***

A.2 Veiligheid

De volgende veiligheidsaspecten dienen te allen tijde in acht te worden genomen:

1. **Lees eerst de gebruiksershandleiding alvorens de machine in gebruik te nemen.**
2. **Bediening van de machine is alleen toegestaan door ter zake kundig personeel welke vóór de ingebruikneming is geïnstrueerd door geautoriseerd personeel.**
3. **Door de hoogspanning kan ozon (GIFTIG!) ontstaan. Daarom dient er bij gebruik altijd een puntafzuiging te zijn aangesloten.**
4. **De cabinedeur mag alleen worden geopend en gesloten indien de hoogspanning is afgeschakeld. Indien de deur wordt geopend wanneer de opstelling in bedrijf is zal een noodprocedure in werking treden. Hierbij worden alle voedingen uitgeschakeld en kortgesloten. Hierbij kan mogelijk schade aan de opstelling ontstaan en dient dus te allen tijde te worden voorkomen!**
5. **De opstelling in de cabine mag alleen worden aangepast door geautoriseerd personeel. Het losmaken van de hoogspanningskabels is dan ook verboden voor het bedienend personeel.**
6. **Tijdens het gebruik van de cabine en met name de polymeeroplossingen dient te allen tijde een veiligheidsbril te worden gedragen.**
7. **Het is verboden om kabels of andere voorwerpen door de kabeldoorvoeren te steken wanneer de opstelling in bedrijf is.**
8. **Het ventilatierooster aan de voorzijde en de ventilator aan de achterzijde mogen nooit worden afgedekt.**

A.3 Inbedrijfstelling

De inbedrijfstelling dient te gebeuren door ter zake kundig personeel!
Voordat de machine in bedrijf kan worden genomen dient eerst een puntafzuiging te worden aangebracht. Hierna kan de electra op het lichtnet worden aangesloten (230V AC).

Figure A.1: E-spincabine met de rode pijl bij de afzuigopening.

Figure A.2: inschakelpaneel met van links naar rechts: de hoofdschakelaar, power ON indicatielamp en hoogspanning ON indicatielamp.

De cabine moet worden ingeschakeld via de hoofdschakelaar aan de voorzijde. Het Power lampje zal gaan branden en het operator panel zal opstarten. Aan de achterzijde zal automatisch de koelventilator worden gestart. Aan de rechterzijde van het paneel zitten nog enkele additionele connectoren. Momenteel wordt alleen de bovenste gebruikt voor de aansturing van een infusion pump.

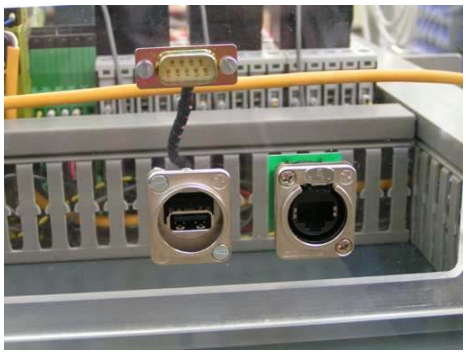

Figure A.3: connectoren met aan de bovenzijde de infusion pump aansluiting (TTL) en beneden van link naar rechts een USB en een Ethernet aansluiting. Deze twee connectoren zijn momenteel nog niet in gebruik.

Aan de achterzijde van de cabine is een grote "brievenbus" sleuf aangebracht voor de doorvoer van de aansluitkabels van de opstellingen die in de cabine worden geplaatst. De sleuf kan aan de binnenzijde worden verhoogd om de doorvoer van grotere stekker mogelijk te maken. De sleuf dient echter voor de ingebruikneming weer volledig naar beneden te worden teruggezet!
Aan de beide zijkanten zijn nog gaten aanwezig voor de doorvoer van oplosmiddelen en gassen. Indien een van de gaten niet wordt gebruikt dient deze met de bijgeleverde stop te worden afgesloten.

A.4 Gebruik

De opstelling wordt bediend via het bedieningspaneel. Het paneel heeft twee hoofdlijnen, namelijk manuele bediening en tijd gestuurde doorloop. De manuele modus dient voor het handmatig schakelen van de pomp en de hoogspanning. De timed operation omvat een klokbesturing van de cabine waarbij de pomp en de hoogspanning via ingegeven tijdstappen kunnen worden aangestuurd.
Na het inschakelen van de cabine start het bedieningspaneel op en wordt na de opstartprocedure het hoofdscherm weergegeven (zie de figuren op de volgende bladzijde). In het hoofdscherm kan de gewenste spanning worden ingegeven bij `HV U SP [kV]` via de numerieke toetsen. De ingevulde waarde dient in kiloVolts te zijn. Niet gehele waarden kunnen worden ingegeven met een KOMMA ertussen. De waarde wordt pas daadwerkelijk ingevoerd na het drukken van de ENTER toets. In het hoofdscherm wordt naast het voltage ook de stroom (`HV I PV [nA]`) weergegeven die tussen de aansluitingen van de hoogspanning aanwezig is. Deze waarde wordt weergegeven in nano ampères. Onderaan in het hoofdscherm staat de inwendige temperatuur van de cabine weergegeven. Deze waarde wordt in graden Celcius weergegeven. Indien de deur van de cabine geopend is zal er `DOOR OPEN!` knipperen in plaats van de weergave van de temperatuur.
Via de `F1` toets komt men in het tijdinstelling scherm. Hier kan wederom via de numerieke toetsen en ENTER de gewenste waarde worden ingegeven. De waarde dient in seconden te worden ingegeven! `Pre-pump time` staat voor het aantal seconden dat de pomp wordt aangezet voordat de hoogspanning wordt ingeschakeld. `HV on time` staat voor de tijd dat de hoogspanning en de pomp samen in bedrijf zijn. `HV off delay` staat voor de tijd dat de hoogspanning ingeschakeld blijft nadat de pomp is uitgeschakeld. Via de pijltjestoetsen kunnen de verschillende velden worden geselecteerd. Na het drukken van de `F1` toets komt men weer terug in het hoofdscherm.
Via de `K1` toets kan de pomp manueel worden in- en uitgeschakeld en via de `K2` toets kan de hoogspanning worden aan- en afgekoppeld. De `K3` toets start de timed operation procedure. Links onder in het scherm wordt de doorloop van de procedure dan weergegeven. In geval van een fout kan de timed operation procedure worden onderbroken door de `K4` toets te drukken!

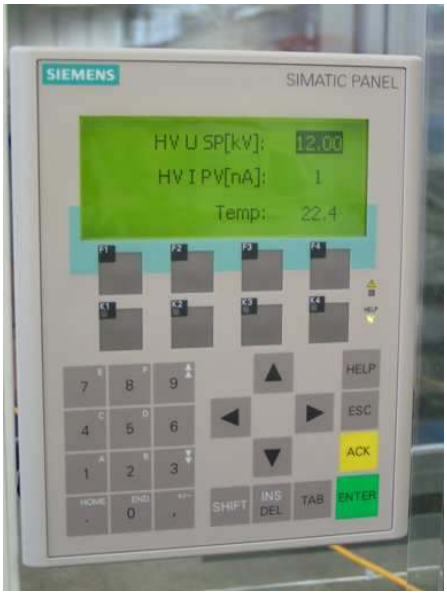

Figure A.4: Hoofdscherm

Figure A.5: Tijdinstelling scherm

A.5 Onderhoud en werkzaamheden

Het apparaat dient voor het plegen van onderhoud en/of werkzaamheden spanningsloos te worden gemaakt. Hiervoor dient de stekker uit het stopcontact te worden gehaald. Het onderhoud of de aanpassing van de opstelling mag alleen gebeuren door geautoriseerd personeel!

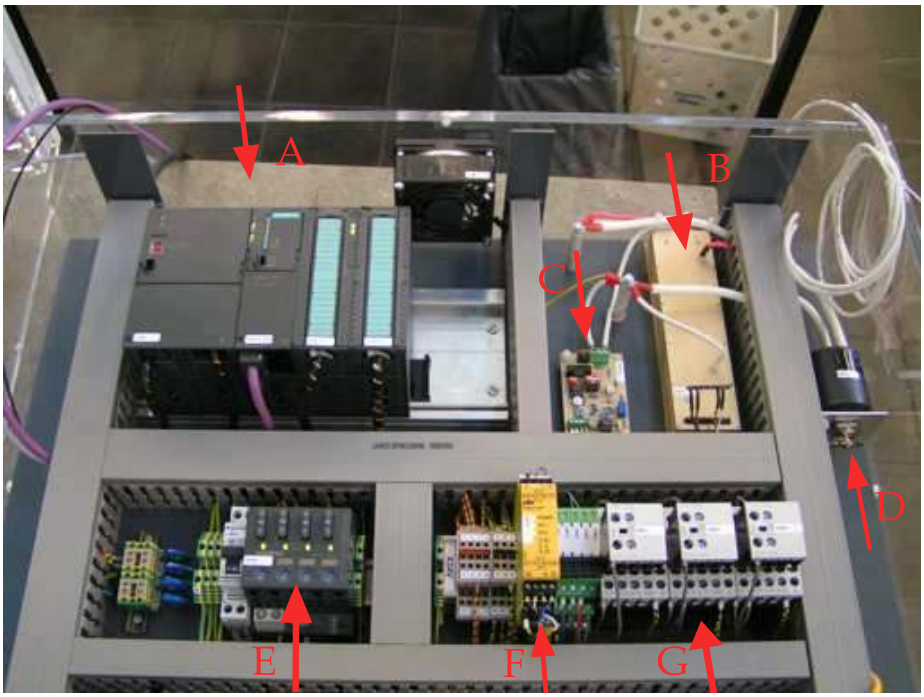

Figure A.6: Elektrisch gedeelte onder de cabine met de volgende componenten: (A) voeding/PLC, (B) Hoogspanningsvoeding, (C) Stroom meting printplaat, (D) Hoogvoltage relais, (E) Digitale voeding distributie, (F) Deur beveiliging en (G) Schakelrelais.

A.6 Preventief onderhoud

De cabine dient jaarlijks een preventieve onderhoudsbeurt te ondergaan. Dit kan geschieden door de Gemeenschappelijke Technische Dienst. Het onderhoud dient gericht te zijn op:

- Stof
- Veroudering en kristallisatie bekabeling
- Controle netsnoeren
- Functionele test

In het constructiedossier is een keuringsrapport opgenomen met de opvolgende gewenste keuringsdatum. **De 1e keuring dient te geschieden binnen 1 jaar na de afgifte van de CE verklaring.**

B

Relaxation routine description

In Relaxation the ODE's have to be replaced by approximate finite difference equations (FDE's) on a mesh of points that covers the integration domain. One way to turn an ODE into an FDE is an algebraic equation, relating function values at two points $k, k-1$ [37]:

$$y_k - y_{k-1} - (x_k - x_{k-1})g[\frac{1}{2}(x_k + x_{k-1}), \frac{1}{2}(y_k + y_{k-1})] = 0 \tag{B.1}$$

The problem involves N coupled first-order ODE's represented by FDE's on a mesh of M points. Then the solution consists of values for N dependent functions given at each of the M mesh points, or $N \times M$ variables in all. The relaxation method determines the solution by starting with a guess and improving it, iteratively. During the iterations the solution is improved and the result *relaxes* towards the true solution.
The N coupled first-order equations satisfy n_1 boundary conditions at x_1 (initial boundary) and $n_2 = N - n_1$ boundary conditions at x_M (final boundary). In general, a uniform grid is chosen on the interval of $k = 1, 2, \ldots, M$ points at which values for the independent variable x_k are supplied.
The notation $\mathbf{y}_k$ is used to refer to the entire set of dependent variables $y_1, y_2, \ldots, y_N$ at point x_k. In the middle of the mesh, at an arbitrary point k the set of first-order ODE's can be approximated by algebraic relations of the form

$$0 = \mathbf{E}_k \equiv \mathbf{y}_k - \mathbf{y}_{k-1} - (x_k - x_{k-1})\mathbf{g}_k(x_k, x_{k-1}, \mathbf{y}_k, \mathbf{y}_{k-1}), \quad k = 2, 3, \ldots, M \tag{B.2}$$

the notation signifies that $\mathbf{g}_k$ can be evaluated using information from both points $k, k-1$. N equations coupling $2N$ variables at points $k, k-1$ are provided by $\mathbf{E}_k$ (FDE's). These FDE's provide a total of $(M-1)N$ equations for MN unknowns. The remaining N equations come from the boundary conditions.
The initial boundary applies

$$0 = \mathbf{E}_1 \equiv \mathbf{B}(x_1, \mathbf{y}_1) \tag{B.3}$$

The final boundary applies

$$0 = \mathbf{E}_{M+1} \equiv \mathbf{C}(x_M, \mathbf{y}_M) \tag{B.4}$$

$\mathbf{E}_1$ and $\mathbf{B}$ only have nonzero components which correspond to the n_1 boundary conditions. These components should be placed at the end of the vectors. At the other boundary only the first n_2 components of $\mathbf{E}_M + 1$ and $\mathbf{C}$ are nonzero.
The solution to the FDE problems can be obtained by determining increments $\triangle y_{j,k}$ in such a way (starting from an initial guess for $y_{j,k}$) that $y_{j,k} + \triangle y_{j,k}$ is an improved approximation to the solution.
Equations for the increments can be developed by expanding the FDE's in first-order Taylor series with respect to small changes $\triangle \mathbf{y}_k$. For $k = 2, 3, \ldots, M$ this gives

$$\begin{aligned}\mathbf{E}_k(\mathbf{y}_k + \triangle\mathbf{y}_k, \mathbf{y}_{k-1} + \triangle\mathbf{y}_{k-1}) \approx \mathbf{E}_k(y_k, y_{k-1}) + \\ \sum_{n=1}^{N} \frac{\partial \mathbf{E}_k}{\partial y_{n,k-1}} \triangle y_{n,k-1} + \sum_{n=1}^{N} \frac{\partial \mathbf{E}_k}{\partial y_{n,k}} \triangle y_{n,k}\end{aligned} \tag{B.5}$$

$$\sum_{n=1}^{N} S_{j,n} \triangle y_{n,k-1} + \sum_{n=N+1}^{2N} S_{j,n} \triangle y_{n-N,k} = -E_{j,k}, \quad j = 1, 2, \ldots, N \tag{B.6}$$

where

$$S_{j,n} = \frac{\partial E_{j,k}}{\partial y_{n,k-1}}, \quad S_{j,n+N} = \frac{\partial E_{j,k}}{\partial y_{n,k}}, \quad n = 1, 2, \ldots, N \tag{B.7}$$

The quantity $S_{j,n}$ is an $N \times 2N$ matrix at each point k. Each interior point supplies a block of N equations coupling $2N$ corrections to the solution variables at the points $k, k-1$. Similarly, the algebraic relations at the boundaries can be expanded in first-order Taylor series.
Now a set of linear equations is complete to be solved for the corrections $\triangle \mathbf{y}$, which can be iterated until the corrections are sufficiently small.
To minimize the total number of operations the equations are adapted by Gaussian elimination. This procedure consists of manipulating the equations by elementary operations such as dividing rows of coefficients by a common factor to produce unity in diagonal elements, and adding appropriate multiples of other rows to produce zeros below the diagonal. Once the elimination procedure is completed, the solution follows by doing a backsubstitution procedure.
The whole procedure only attempts itmax correction cycles before quitting, even if the solution has not converged. Each inversion of the matrix produces corrections. These have to become smaller as the iterations proceed. When the remaining error is smaller than the desired convergence value, the method has converged.

B.1 Model implementation

For simplicity we take a uniform grid on the interval $0 \leq z \leq \chi$. For M meshpoints we have:

$$h = \frac{1}{M-1} \tag{B.8}$$

$$x_k = (k-1)h, \quad k = 1, 2, \ldots, M \tag{B.9}$$

At interior points $k = 2, 3, \ldots, M$,equation (5.24) gives

$$E_{1,k} = y_{1,k} - y_{1,k-1} - \frac{h}{2}(y_{3,k} + y_{3,k-1}) \tag{B.10}$$

equation (5.25) gives

$$E_{2,k} = y_{2,k} - y_{2,k-1} - \frac{h}{2}(y_{4,k} + y_{4,k-1}) \tag{B.11}$$

equation (5.26) gives

$$\begin{aligned} E_{3,k} = {} & \frac{6\eta}{hRe}(y_{3,k} - y_{3,k-1}) - \frac{y_{3,k} + y_{3,k-1}}{\frac{1}{4}(y_{1,k} + y_{1,k-1})^2} - \frac{\frac{1}{4}(y_{1,k} + y_{1,k-1})(y_{3,k} + y_{3,k-1})}{We} \\ & - \frac{\frac{3}{2}\eta(y_{3,k} + y_{3,k-1})^2}{\frac{1}{2}Re(y_{1,k} + y_{1,k-1})} + \frac{3\dot{\eta}(y_{3,k} + y_{3,k-1})}{Re} - \frac{\frac{1}{8}(y_{1,k} + y_{1,k-1})^3}{Fr} \\ & - \frac{\frac{1}{2}\beta\varepsilon(y_{2,k} + y_{2,k-1})}{\frac{1}{4}(y_{1,k} + y_{1,k-1})^2}\Big(\frac{1}{4}(y_{1,k} + y_{1,k-1})(y_{4,k} + y_{4,k-1}) \\ & - \frac{1}{4}(y_{2,k} + y_{2,k-1})(y_{3,k} + y_{3,k-1})\Big) \\ & - \frac{2\varepsilon}{Pe}\frac{1}{4}(y_{1,k} + y_{1,k-1})(y_{2,k} + y_{2,k-1})\big(1 - \frac{1}{2}(y_{2,k} + y_{2,k-1})\big) \end{aligned} \tag{B.12}$$

finally, equation (5.27) gives

$$\begin{aligned} E_{4,k} = {} & \frac{\beta}{2h}(y_{4,k} + y_{4,k-1}) - \frac{1}{ln(\chi)}\Big(\frac{\frac{1}{2}(y_{2,k} + y_{2,k-1})}{\frac{1}{4}(y_{1,k} + y_{1,k-1})} - E_\infty\Big) \\ & - \frac{1}{Pe}\Big(\frac{1}{2}(y_{1,k} + y_{1,k-1})(y_{3,k} + y_{3,k-1}) - \frac{1}{4}(y_{1,k} + y_{1,k-1})^2(y_{4,k} + y_{4,k-1}) \\ & - \frac{1}{4}(y_{1,k} + y_{1,k-1})(y_{2,k} + y_{2,k-1})(y_{3,k} + y_{3,k-1})\Big) \end{aligned} \tag{B.13}$$

The matrix of partial derivatives $S_{i,j}$ is defined with i the equation and j the variable. j runs from 1 to 4 at $k-1$ and from 5 to 8 for y_j at k. Now by stating equation (5.26) as $f3$ and equation (5.27) as $f4$ with $yi = \frac{1}{2}(y_{i,k} + y_{i,k-1})$ for $i = 1, 2, 3, 4$ the partial derivatives can be derived as:

$$\begin{aligned} df3d1 = &-4y3/y1^3 + y3/We - 6\eta/Re \cdot (y3/y1)^2 + 3y1^2/Fr \\ &+ \beta\varepsilon y2/y1^3 \cdot (4y2y3 - y1y4) \\ &+ \varepsilon/Pe^2 \cdot (1-y2)y1^3 \cdot (4y3 - 5y1y4 - 4y2y3) \\ &+ 2\varepsilon/Pe \cdot y2(1-y2) \end{aligned} \tag{B.14}$$

$$\begin{aligned} df3d2 = &\beta\varepsilon/y1^2 \cdot (y1y4 - 4y2y3) + \varepsilon/Pe^2 \cdot y1^4 \cdot (y1y4 + 2y2y3 - 2y3) \\ &+ 2\varepsilon/Pe \cdot y1(1-2y2) \end{aligned} \tag{B.15}$$

$$\begin{aligned} df3d3 = &2/y1^2 + y1/We + 12\eta/Re \cdot y3/y1 - 6\dot{\eta}/Re - 2\beta\varepsilon(y2/y1)^2 \\ &+ \varepsilon/Pe^2 \cdot y1^4 \cdot (1-y2)^2 \end{aligned} \tag{B.16}$$

$$df3d4 = \beta\varepsilon y2/y1 - \varepsilon/Pe^2 \cdot y1^5 \cdot (1-y2) \tag{B.17}$$

$$df4d1 = -2/ln(\chi) \cdot y2/y1^3 + 2/Pe \cdot (y3 - y1y4 - y2y3) \tag{B.18}$$

$$df4d2 = 1/ln(\chi)y1^2 - 2y1y3/Pe \tag{B.19}$$

$$df4d3 = 2y1(1-y2)/Pe \tag{B.20}$$

$$df4d4 = -y1^2/Pe \tag{B.21}$$

Now equation (B.10) gives

$$\begin{aligned} &S_{1,1} = -1, \quad S_{1,2} = 0, \quad S_{1,3} = -\frac{h}{2}, \quad S_{1,4} = 0 \\ &S_{1,5} = 1, \quad S_{1,6} = 0, \quad S_{1,7} = -\frac{h}{2}, \quad S_{1,8} = 0 \end{aligned} \tag{B.22}$$

equation (B.11) gives

$$\begin{aligned} &S_{2,1} = 0, \quad S_{2,2} = -1, \quad S_{2,3} = 0, \quad S_{2,4} = -\frac{h}{2} \\ &S_{2,5} = 0, \quad S_{2,6} = 1, \quad S_{2,7} = 0, \quad S_{2,8} = -\frac{h}{2} \end{aligned} \tag{B.23}$$

equation (B.12) gives

$$\begin{aligned} &S_{3,1} = -\frac{df3d1}{2}, \quad S_{3,2} = -\frac{df3d2}{2}, \quad S_{3,3} = \frac{-6\eta}{hRe} - \frac{df3d3}{2}, \quad S_{3,4} = -\frac{df3d4}{2} \\ &S_{3,5} = -\frac{df3d1}{2}, \quad S_{3,6} = -\frac{df3d2}{2}, \quad S_{3,7} = \frac{6\eta}{hRe} - \frac{df3d3}{2}, \quad S_{3,8} = -\frac{df3d4}{2} \end{aligned} \tag{B.24}$$

and equation (B.13) gives

$$\begin{aligned} &S_{4,1} = -\frac{df4d1}{2}, \quad S_{4,2} = -\frac{df4d2}{2}, \quad S_{4,3} = -\frac{df4d3}{2}, \quad S_{4,4} = -\frac{\beta}{2h} - \frac{df4d4}{2} \\ &S_{4,5} = -\frac{df4d1}{2}, \quad S_{4,6} = -\frac{df4d2}{2}, \quad S_{4,7} = -\frac{df4d3}{2}, \quad S_{4,8} = \frac{\beta}{2h} - \frac{df4d4}{2} \end{aligned} \tag{B.25}$$

At z=0 the following boundary conditions are present

$$E_{3,1} = y_{1,k} - 1 \tag{B.26}$$
$$E_{4,1} = y_{2,k} - E_0 \tag{B.27}$$

Now the nonzero components of $S_{3,j}$ and $S_{4,j}$ are

$$S_{3,5} = 1 \tag{B.28}$$
$$S_{4,6} = 1 \tag{B.29}$$

At z=χ the boundary conditions are

$$E_{1,M+1} = y_{1,M} + 4\chi y_{3,M} \tag{B.30}$$
$$E_{2,M+1} = y_{2,M} - E_\infty y_{1,M}^2 \tag{B.31}$$

This leads to the nonzero components of $S_{1,j}$ and $S_{2,j}$

$$S_{1,5} = 1 \tag{B.32}$$
$$S_{1,7} = 4\chi \tag{B.33}$$
$$S_{2,5} = -2E_\infty y_{1,M} \tag{B.34}$$
$$S_{2,6} = 1 \tag{B.35}$$